DEVELOPMENT OF SHEAR STRESS MEASUREMENT TECHNIQUE AND PLOTTING SURFACE STREAK LINES USING OIL TECHNIQUE

by

Syed Shoiab

A Thesis

Submitted to the Faculty of Purdue University

In Partial Fulfillment of the Requirements for the degree of

Master of Science in Aeronautics and Astronautics

School of Aeronautics and Astronautics

West Lafayette, Indiana

August 2021

THE PURDUE UNIVERSITY GRADUATE SCHOOL
STATEMENT OF COMMITTEE APPROVAL

Dr. Guillermo Paniagua
School of Mechanical Engineering

Dr. Sally Bane
School of Aeronautics and Astronautics

Dr. Terrence R. Meyer
School of Mechanical Engineering

Approved by:
Dr. Gregory A. Blaisdell

Dedicated to my family and friends.

ACKNOWLEDGMENTS

The author would like to thank Dr. Guillermo Paniagua and Dr. Iman Rahbari for the timely guidance in the fulfillment of this thesis work. The author expresses his gratitude to Dr. Sally Bane for permitting to test in the arms wind tunnel facility. The author would like to thank Dr. Terrence R. Meyer for their support throughout this project. The author would also like to thank Antoni Rebassa Torrens for allowing me to test in their test article. The author appreciates the help from colleagues and friends that helped in bringing this thesis to light.

TABLE OF CONTENTS

LIST OF TABLES

LIST OF FIGURES

NOMENCLATURE

SYMBOLS

x	x- direction
y	y- direction
z	z- direction
U_c	Convectional velocity
P	Pressure
L	Deformed droplet length
h	Droplet height
u	X-direction velocity component
τ	Shear stress
σ	Surface tension
μ	Dynamic viscosity
ρ	Density
ν	Kinematic viscosity
δ	Boundary layer thickness
g	Gravity
t	Time
s	Deformed droplet slope

ABBREVIATIONS

UV	Ultraviolet
FOV	Field Of View
ROI	Region Of Interest
SACOC	Surface Air Cooled Oil Cooler
PETAL	Purdue Experimental Turbine Aerothermal Laboratory
LEAF	Linear Experimental Aerothermal Facility
AOA	Angle Of Attack

ABSTRACT

Wall shear stress is an important parameter in accessing the aerodynamics performance of an object. With the race to optimize the performance of an aerodynamic body, multiple shear stress measurements have been developed such as OFI (Oil Film Interferometry), MEMS (Microelectromechanical Sensors), Hotwire, Preston tube, Hot films, etc. where most of these techniques are expensive or intrusive. In the experimental measurement techniques, the complexities and intrusiveness often play a major role in selecting a measurement technique.

Hence the developed shear stress measurement technique is simple yet effective to obtain accurate shear stress results using oil. The secondary challenge faced in the aerodynamic experiments is to obtain a flow visualization. The developed shear stress measurement technique is expanded to obtain the qualitative and quantitative flow development data around the ROI. The developed methodology relies on the thin film assumption where the droplet is sufficiently thin such that the gravity, pressure, and surface tension forces acting on the droplet are not significant, and the droplet is deformed only under the significant shear stress forces. This technique assumes constant shear stress along the deformed droplet, at regions of high shear gradient this technique can be employed using smaller droplets applied at the constant shear regions. The viscosity of the oil used must be chosen accordingly to the test conditions to obtain a constant thinning rate for a substantial amount of time. Finally, the droplet deformation is tracked using a camera and the thinning rate of the droplet is computed using an image processing tool developed.

The obtained results are compared with the theoretical results for a flat plate and with the CFD results for the SACOC testing. The technique was tested in a range of test conditions with a low subsonic of 20m/s to a compressible flow of Mach 0.3 and Mach 0.5. Uncertainty estimation is performed to recognize the confidence level of the developed technique.

Developed measurement technique clubs two different measurements, shear stress, and qualitative and quantitative flow viz, acquiring the data for both in a single test, thereby reducing the repeatability of experiments, resources, and computational power. Moreover, the resources required for this technique are easily available at a low cost and is very simple to implement.

1. INTRODUCTION

1.1 Techniques to measure shear stress and characterize streak lines

As the human nature tends to visualize and experience any phenomenon in life, flow visualization is one of the major aspects of aerospace applications. Over years a vast variety of flow visualization techniques have been developed such as Schlieren, PIV (Particle Image Velocimetry), oil technique, smoke flow visualization, tuft flow, dye method, etc. Even though a plethora of techniques have been developed for flow visualization, it is still challenging to visualize the flow at the critical enclosed locations and to characterize the primary and secondary flows.

Hydrogen bubble and dye visualization are usually used in water tunnels where a streak of dye is introduced into the water tunnel and it forms a streak line pattern around the object in the water tunnel whereas, in the hydrogen bubble technique a DC voltage applied to the electrode upstream the model which electrolysis the water and generates small hydrogen bubbles which are then swept by the flow and forming streak lines around the model. G.R.Offen [1] coupled dye and hydrogen bubble technique to visualize the turbulent boundary layer over a flat plate.

In Particle Image Velocimetry the tagged particles are introduced into the flow stream and are tracked. [2] shows the FLEET demonstration in a bladeless turbine in conjunction with Schlieren used to decipher the flow physics over the wavy test section.

The different methodologies adapted to measure shear stress include Oil Film Interferometry (OFI), Microelectromechanical Sensors (MEMS), hot films, etc. The OFI is most exclusively used in measuring shear stress, is discussed in [illegible] which utilizes the fringes formed by the oil upon deformed by the airflow to calculate the shear stress. The hot films work on ‘hot wire’ principle to measure the shear stress over the surface it is applied on.measure the shear stress over the surface it is applied on.

1.2 Research Objectives

Shear stress measurement is an essential element in the aero industry. It is extremely important to access the skin friction in order to determine the drag acting on an aerodynamic body. To access the performance, skin friction measurements are also widely used in the automotive

industry and hence remarkable developments have been made in the development of shear stress measurement techniques.

Flow visualization has always been exciting although characterization of flow is always a challenging task. However, visualizing the flow in real-time would help in tracking the movement of the oil droplets in time which can further be plotted to obtain the quantitative data.

This project is focused on the development of a shear stress measurement technique that is further extended to obtain flow behavior by plotting surface streak lines. This technique is demonstrated with the help of illuminating oil droplets deposited on the surface of interest and tracked in time with a high-speed camera. Image processing is implemented to track the thinning rate of the droplet which also provides a piece of evidence on flow behavior. The primary focus of this project is to club the two independent measurement techniques, therefore obtaining data for both the techniques simultaneously in a single run, reducing the errors due to repeatability and since the same equipment are used for both the measurement techniques, this provides flexibility to perform multiple optical measurements alongside. Therefore, the objectives of this research can be summarized as follows:

1. Development of shear stress measurement technique
2. Deriving qualitative and quantitative flow behavior data, employing surface streak lines to characterize secondary flows
3. Experimental demonstration and validation for developed methodology

1.3 Research Methodology

This work is focused on the development of a technique to measure the wall shear stress which is further extended to plot surface streak lines by data processing. The method is based on the oil technique and since the oil is readily available, easy to implement, this technique proves advantageous comparatively to other expensive shear stress measurement techniques, such as optical sensors, hot films, mems, etc.

1.3.1 Development of Shear stress measurement technique

Silicone based oil is used in this experimental campaign mixed with a small amount of fluorescence pigment to enhance the illuminance of the oil with respect to the background. This is

essential in order to accurately detect the boundaries of the oil droplet. Different coloring pigments have been tried to obtain the best illumination. A variety of silicone oils with different viscosities are considered and based on the test conditions, the most suitable oil viscosity has been chosen. The viscosity of the oil-pigment mixture used is determined with a rotating based Anton Paar rheometer. Experiments are performed at Zucrow Labs and arms wind tunnel facility, Purdue University.

Small droplets of oil mixture are applied on the surface of interest. The oil is tracked with a high-speed camera in time and the obtained frames are processed to extract the area of the droplet which is further solved based on droplet shape assumption to obtain the height of the droplet, therefore, obtaining the droplet thinning rate. Determining the slope of the line from thinning rate vs time, and with the knowledge of viscosity of the oil used, the surface shear stress is calculated.

1.3.2 Plotting Streak lines

Identifying secondary flows around a complex structure is challenging as the flow behavior is unpredictable and usually identifying the flow direction especially around a vortex is tiresome.

The tracked droplets can be used to plot the surface streak lines. A matrix of droplets is applied on the surface and only a few are used to calculate the shear stress and all droplets are used to plot the surface streak lines to obtain the flow behavior. Tracking in time helps to identify the flow direction and visualize the flow behavior in real-time as this measurement technique is associated with the shear stress technique and the data procurement is done simultaneously.

Oil droplets are tracked using MATLAB image processing and temporal and special deformation of the oil droplets is obtained from which the flow behavior is inferred, and surface streak lines are plotted by mapping the image to real-world coordinates using a camera calibration matrix with the help of multiple calibration images. The streak lines tracked provide detailed information of flow behavior at the walls and help us to characterize secondary flows including separation and reattachment points in the flow, provide detailed information of flow behavior at the walls and help us to characterize secondary flows including separation and reattachment points in the flow.

This technique comes in handy in simple diagnosis to identify if the flow separates over a surface and since it is achieved using oil and some coloring pigment, it is relatively cheap, easily

accessible, and considerably simple to implement. All one needs is a test section with optical access and a surface suitable to apply oil over it.

1.4 Thesis guideline

This thesis is divided into 4 chapters. The first chapter (Chapter 2), discusses the theory involved in the developed shear stress methodology, addressing the different calibration processes adapted, implied assumptions, developed data processing routine to obtain the shear stress calculations off the surface, concluding the chapter with uncertainty quantification involved in shear stress measurements. Chapter 3 outlines the post processing routine adapted to plot the surface streak lines.

Chapter 4 is allotted to demonstrate the experimental setup and results obtained and discussion. The final chapter (Chapter 5) discusses the conclusions of this thesis findings.

2. DEVELOPMENT OF SHEAR STRESS MEASUREMENT TECHNIQUE

2.1 Thin Film Theory

Thin film theory is the basis of the methodology used for the shear stress measurement technique. This theory was first studied by Squire [4] where they obtained the mathematical solution for motion of thin oil sheet of non uniform thickness and concluded that the oil tends to predict the separation point early than the actual separation region and that the oil flows in the direction of boundary layer skin friction. The author also concluded that the effect of oil flow in the boundary layer is negligible in the boundary layer fluid motion and these conclusions are independent of oil viscosity. These provided a building block for the shear stress measurement technique using oil which was then studied by Thanner et.al [5] in depth deriving equations for oil thinning under different conditions. Thanner conducted a variety of experiments on oil under the effect of gravity, rotation and, wind tunnel and reported that the oil drop deposited on the solid surface is acted on by the shear stress, pressure gradient generated due to airflow over the surface, acceleration of the surface (if any), surface tension and gravity. However, for general application, the effect due to gravity, surface tension and acceleration of the surface can be neglected, but as most of the experiments are conducted in the wind tunnel it is important to study further the effect of pressure gradient on the thin film oil surface.

[6] in their project report have provided a detailed analysis on the forces acting on the oil droplet and have concluded that all other forces acting on the droplet are at least one order of magnitude lesser than the shear stress acting on the droplet. In order to understand this better a control volume analysis is performed by the author as follows:

Assuming the droplet deforms along x direction and that the thickness of the droplet in the z direction (where z going into the page) remains constant, one can derive the equations in 1D. Since, the droplet deforms in due to the shear induced by the sir flow flowing in x-direction, this assumption seems reasonable.

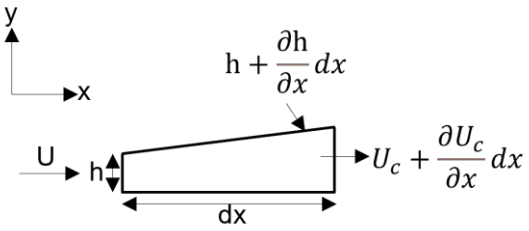

Figure 2-1: Assumed shape for control volume analysis

From Figure 2-1 continuity equation in one dimension can be written as 2. 1 where U_c is the convective velocity defined as 2. 2 and the x-momentum equation is written as 2. 3.

$$\frac{\partial h}{\partial t} + \frac{\partial (hU_c)}{\partial x} = 0 \qquad 2.\ 1$$

$$U_c \equiv \frac{1}{h}\int_0^h u dy \qquad 2.\ 2$$

$$\rho\left(\frac{\partial u}{\partial t} + u\frac{\partial u}{\partial x} + v\frac{\partial u}{\partial y} + w\frac{\partial u}{\partial z}\right) = -\frac{\partial P}{\partial x} + \mu\left(\frac{\partial^2 u}{\partial x^2} + \frac{\partial^2 u}{\partial y^2} + \frac{\partial^2 u}{\partial z^2}\right) + \rho g_x \qquad 2.\ 3$$

2. 3 can further be simplified for 1D assumption and neglecting the viscous terms in y-z direction and inertial terms and simplifying 2. 4 is obtained where the term denoted in parenthesis is nothing but the shear stress in x direction. Furthermore, 2. 4 is integrated twice to obtain the velocity in x-direction with the boundary condition that the velocity is continuous at air/oil interface and the viscous stresses are zero at the solid boundary and are equal at air/oil interface. The velocity in x-direction is integrated again in y in between wall and oil surface to get the convective velocity 2. 5.

$$0 = -\frac{\partial P}{\partial x} + \frac{\partial}{\partial y}\left(\mu\frac{\partial u}{\partial y}\right) + \rho g_x \qquad 2.\ 4$$

$$U_c = \frac{1}{h}\int_0^h u\mathrm{d}y = \frac{\tau_{w,x} h}{2\mu} - \frac{h^2}{3\mu}\left(\frac{\partial P}{\partial x} - \rho g_x\right) \qquad 2.\ 5$$

The pressure within the oil film can be denoted as 2.6 from Naugton [7] where P_o is the pressure within the oil film that differs from aerodynamic pressure P acting on the film, this effect is due to the surface tension of the droplet and $\partial^2 h/\partial x^2$ and $\partial^2 h/\partial z^2$ are the curvatures of oil height in x and z direction respectively.

$$P_0 \approx P - \sigma\left(\frac{\partial^2 h}{\partial x^2} - \frac{\partial^2 h}{\partial z^2}\right) \qquad 2.6$$

Now substituting 2. 6 in 2. 5 and plugging in the convective velocity in continuity equation (2. 1) we have:

$$\frac{\partial h}{\partial t} + \frac{\partial}{\partial x}\left\{\frac{\tau_{w,x} h^2}{2\mu} - \frac{h^3}{3\mu}\left[\frac{\partial P}{\partial x} - \frac{\partial}{\partial x}\left(\sigma\left(\frac{\partial^2 h}{\partial x^2} + \frac{\partial^2 h}{\partial z^2}\right)\right) - \rho g_x\right]\right\} = 0 \qquad 2.7$$

Plugging in the general values of the variables involved, we can obtain an order of magnitude, each of these terms contribute in the above equation. Reynolds number involved is close to zero with the considered variables indicating that the viscous forces are dominating. Variables considered in the analysis are $L = 0.01m$, $h = 0.1mm$, $v = 10^{-5}\ m^2/s$, $\tau_w = 1.37Pa$, $\rho = 970kg/m^3$, $g = 9.81m/s^2$, $\sigma = 0.02N/m$, $\partial P/\partial x = 0$, $\mu = 0.5Pa\text{-}s$, $\Delta x = 1mm$, $\Delta h = 0.02mm$, $U_c = \tau_w h/\rho v$, using these values yield:

Reynolds number:
$$\frac{\text{Inertial force}}{\text{Viscous force}} = \frac{\rho U_c^2/L}{\mu U_c^2/h^2} \approx \frac{\tau_w h^3}{\rho v^2 L} \approx 10^{-8} \qquad 2.8$$

Pressure term:
$$\frac{h^3}{3\mu}\frac{\partial P}{\partial x} = 0 \qquad 2.9$$

Surface tension term:
$$\frac{h^3}{3\mu}\frac{\partial}{\partial x}\left(\sigma\frac{\partial^2 h}{\partial x^2}\right) = O(10^{-19}) \qquad 2.10$$

Gravity term:

$$\frac{h^3}{3\mu}\rho g = O(10^{-9}) \quad (2.11)$$

Shear stress term:

$$\frac{\tau_{w,x}h^2}{2\mu} = O(10^{-8}) \quad (2.12)$$

As evident from the above analysis, the shear stress term is at least one order magnitude higher than any of the above-mentioned term, hence dropping all other terms, the governing equation can be written as:

$$\frac{\partial h}{\partial t} + \frac{\partial}{\partial x}\left(\frac{\tau_{w,x}h^2}{2\mu}\right) = 0 \quad (2.13)$$

2. 13 is the thin film equation governing the evolution of the droplet with time in one dimension. Neglecting the shear stress gradient in x direction, linear solution for 2. 13 can be obtained as 2. 14. Using small droplets such that the shear stress within that area remains constant would further strengthen the assumption made, this was also suggested by [8] and [9].

$$h(x,t) = \frac{\mu x}{\tau_w t} \quad (2.14)$$

In order to use the equation 2. 14, the thickness of the oil droplet should be smaller than the value mentioned by lubrication theory. This equation can be further expanded to yield shear stress using the evolution of drop shape at two different instances of time as 2. 15. Oil film responds to a frequency as high as 10kHz as demonstrated by Murphy [10].

$$\tau_w = \mu\frac{\frac{1}{s_2} - \frac{1}{s_1}}{t_2 - t_1} \quad (2.15)$$

Where ‘s’ is the slope of the oil droplet at a given instance of time as shown in Figure 2-2.

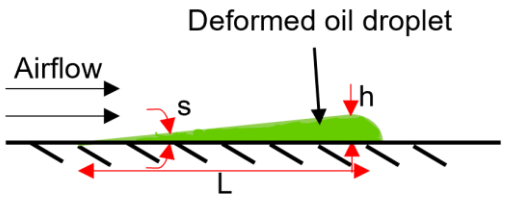

Figure 2-2: Cross section of the deformed oil droplet

However, there are few assumptions required in order for this technique to produce effective results.

1. Pressure can be assumed constant across the deformed oil droplet.
2. Oil is incompressible and has slow viscous motion.
3. Shear stress can be assumed to be in one dimension along which the oil droplet deforms.
4. The height of the oil droplets remains smaller than the air boundary layer thickness.

2.2 Calibration

2.2.1 Theory

Calibration of an image is extremely important in this research campaign as the shear stress measurement completely depends on how accurately the image is mapped onto the real-world dimensions so that the evolution of droplet can be accurately obtained from the frames captured by the camera. In most of the cases, a lens is used as an intermediate between the image sensor and the object, and generally these lenses induce some distortion in the picture, and which can be eliminated by calibrating the camera using a calibration picture. Furthermore, the lens distortion can be classified as radial or tangential distortion.

To calibrate, we need to calculate the intrinsic and extrinsic parameters of the camera and the distortion coefficients which are obtained using multiple calibration images. Additionally, MATLAB offers Camera Calibrator app where one can control certain parameters manually to obtain a better calibration and reduce the calibration errors.

There are two available calibration algorithms offered by MATLAB based on lens used to capture images. A simple pinhole algorithm can be employed if a simple lens is used to capture images, else if a boroscopic lens or Fisheye lens is used to increase the field of view, a fisheye algorithm is also available to undistort images.

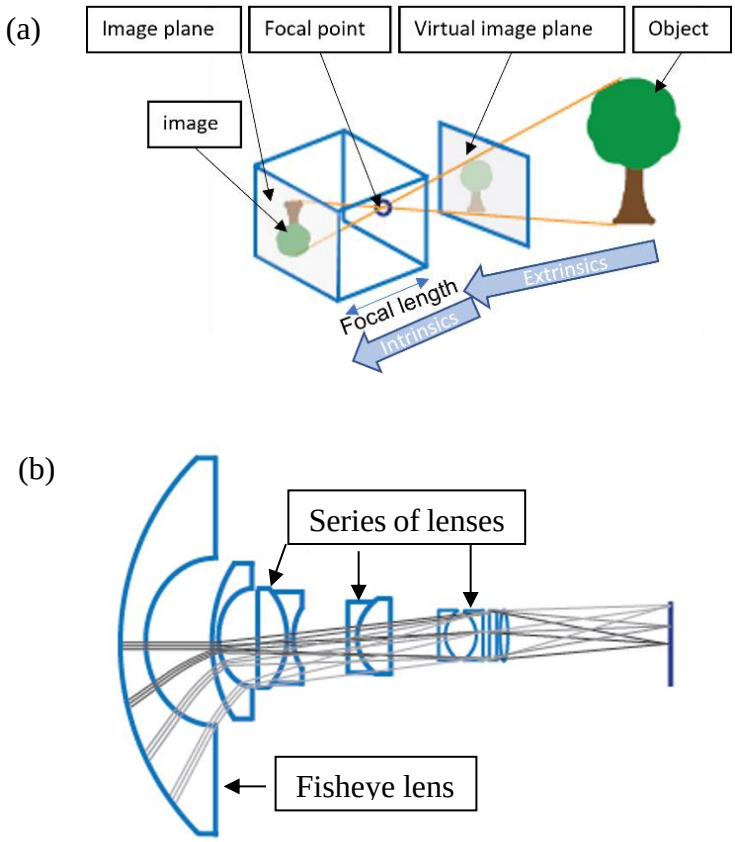

Figure 2-3: Camera models. (a) Pinhole (b) Fisheye

The pinhole calibration model includes, camera model [11] and lens distortion [12] based on the algorithm proposed by Jean-Yves Bouguet [13]. This model does not account for the lens distortion as induced by a fisheye lens. From Figure 2-3(a) and (b) it is observed that a pinhole model does not have a lens and that the fisheye uses a combination of lenses to increase the FOV which results in a high image distortion (a few images are included in the appendix to demonstrate the lens distortion due to fisheye). Since fisheye lens was never used in the experiments conducted in this research study, only pinhole model is considered in this report.

2.2.1.1 Pinhole Camera model

A simple pinhole camera is demonstrated in Figure 2-3(a) and the camera parameters are represented in a 4X3 matrix, which maps the 3D world object onto the image plane. The camera parameters are calculated using the camera intrinsic and extrinsic parameters where the extrinsics

represent the camera location in 3D and intrinsics are the camera parameters such as optical center and focal length.

$$W[x\ y\ 1] = [X\ Y\ Z\ 1]\boldsymbol{P}$$

$$\boldsymbol{P} = \begin{bmatrix} R \\ t \end{bmatrix} K$$

Where, W is the Scale factor, x and y are the 2D image points, X, Y and Z are the 3D world points, P is the camera matrix, K is the intrinsic matrix, the R and t matrix form the camera extrinsics where, R is Rotation and t is translation matrices.

The camera intrinsic matrix K is defined as:

$$\begin{bmatrix} f_x & 0 & 0 \\ s & f_y & 0 \\ c_x & c_y & 1 \end{bmatrix}$$

Where, $[c_x\ c_y]$ — Optical center (the principal point), in pixels,

(f_x f_y) — Focal length in pixels

$f_x = F/p_x$; $f_y = F/p_y$

F — Focal length in world units, typically expressed in millimeters.

(p_x p_y) — Size of the pixel in world units.

s — Skew coefficient, which is non-zero if the image axes are not perpendicular.

$s = f_x \cdot \tan\alpha$

2.2.2 Calibration errors

As mentioned, the pinhole model does not account for any lens distortion, hence in order to account for any lens attached to the image sensor one has to manually account for tangential or rotational errors, both of which are explained below.

2.2.2.1 Tangential error

This error occurs when the lens and image plane are not parallel. Typical examples are cases when the camera had to be tilted to a certain angle to the image plane in order to focus the required FOV.

The distorted points are denoted as $(x_{\text{distorted}}, y_{\text{distorted}})$

$$x_{\text{distorted}} = x + [2^{\star}p_1\ ^{*}x^{*}y + p_2\ ^{*}(r^2 + 2^{*}x^2)]$$

$$y_{\text{distorted}} = y + [p_1 \star (r^2 + 2 * y^2) + 2^{\star}p_2\ ^{\star}x^{\star}y]$$

x, y - Undistorted pixel locations. x and y are in normalized image coordinates. Normalized image coordinates are calculated from pixel coordinates by translating to the optical center and dividing by the focal length in pixels. Thus, x and y are dimensionless.

p_1 and p_2 – Tangential distortion coefficients of the lens.

r^2: $x^2 + y^2$

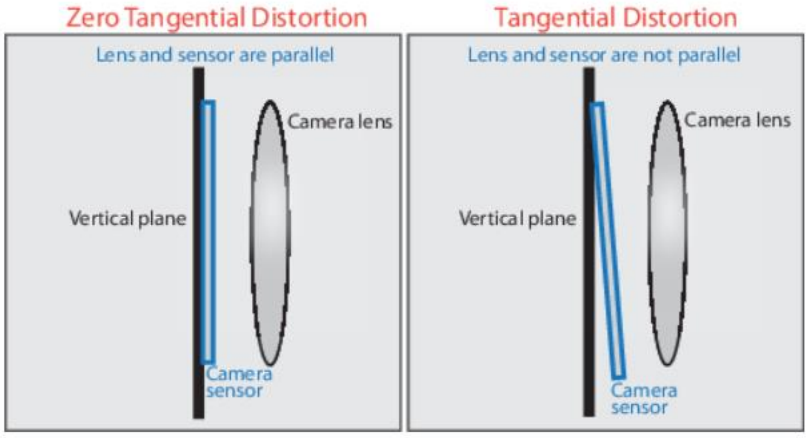

Figure 2-4: Tangential distortion

(Source: https://www.mathworks.com/help/vision/ug/camera-calibration.html)

2.2.2.2 Radial error

Radial distortion occurs in smaller lens, the smaller the lens the grater the distortion. This results in light bending more at the edges than at the optic center.

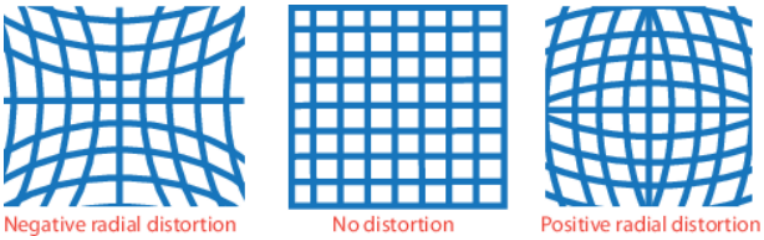

Figure 2-5: Radial distortion
(Source: https://www.mathworks.com/help/vision/ug/camera-calibration.html)

The distortion points are denoted as ($x_{\text{distorted}}$, $y_{\text{distorted}}$)

$$x_{\text{distorted}} = x(1 + k_1^\star r^2 + k_2^\star r^4 + k_3\ ^\star r^6)$$

$$y_{\text{distorted}} = y(1 + k_1^\star r^2 + k_2^\star r^4 + k_3^\star r^6)$$

x, y - Undistorted pixel locations. x and y are in normalized image coordinates. Normalized image coordinates are calculated from pixel coordinates by translating to the optical center and dividing by the focal length in pixels. Thus, x and y are dimensionless.

k_1, k_2, and k_3 - Radial distortion coefficients of the lens.

$r^2: x^2 + y^2$

2.2.3 Calibration Procedure

Camera calibration is obtained using a checkerboard pattern. In practice the real-world dimension of the square used in the checkerboard calibration pattern is known. The MATLAB detects the corner points of each square in the calibration pattern and by just entering the real-world distance between those points, camera coefficient matrix for calibration is obtained. However, it is important to double check the errors associated with the obtained calibration. The calibration seems to be pretty good if the pattern is aligned to the camera lens that is., has less tangential distortion. However, when calibrating a nonlinear surface such as a turbine blade an effort is made to minimize the lens distortion by angling the camera such that the tangential

distortion is negligible, and the errors thus obtained from calibration seem to be pretty reasonable even though the turbine blade surface is not flat.

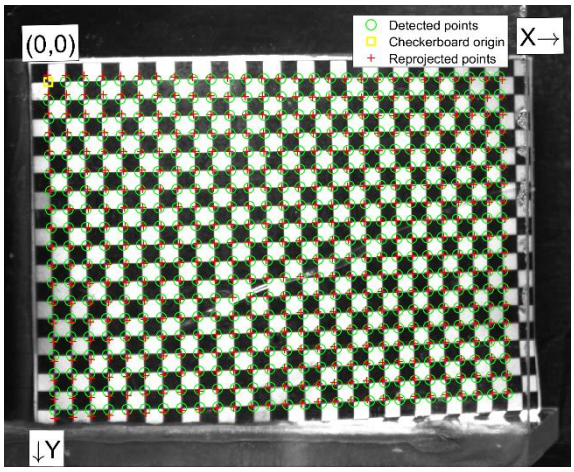

(a)

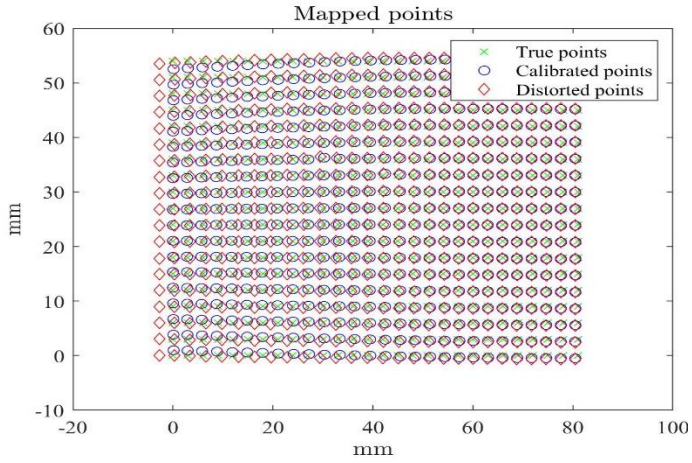

(b)

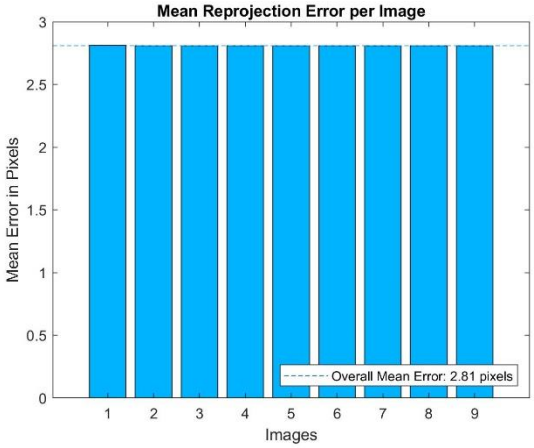

(c)

Figure 2-6: Image calibration (a) Checkerboard calibration image (b) mapped calibration points (c) Corresponding reprojection errors

For calibration minimum of 3 frames are required and as many as 16 calibration images are used for calibration in these tests. Figure 2-6(a) shows one of the raw calibration image. The checkerboard points are detected and are marked in the image, based on the board size entered MATLAB calculates the mean pixel distance between each point and the calculates images are also projected in the figure. The mean reprojection error between the detected points and the reprojected points are shown in Figure 2-6(c). This calibration pattern is fixed on the surface of the turbine and hence we have higher mean projection errors, a comparison case is shown in Figure

2-7 where the calibration pattern was mounted on a flat plate and hence the corresponding projection errors are smaller. With the image points detected by the code and the known distance between each point, camera intrinsic parameters are calculated.

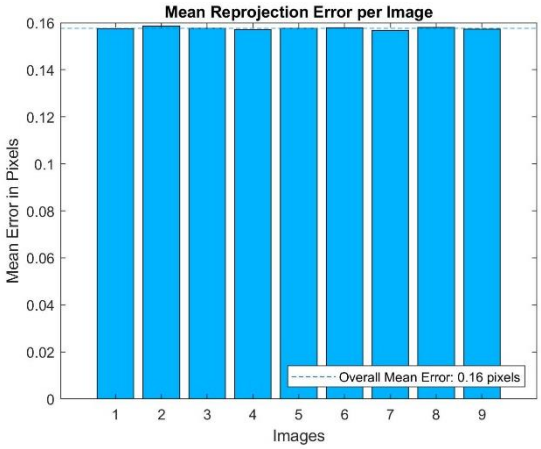

Figure 2-7: Reprojection errors for flat plate calibration

In order to map the detected thinning rate of the droplet it is required to calculate the camera extrinsics. The calibration pattern must be on the surface where the droplet is applied in order to calculate the camera extrinsic matrix at that particular distance from the lens. Using the intrinsic camera parameters computed, the calibration image is undistorted, and the image points obtained from the undistorted image along with the real-world coordinate points the camera intrinsic parameters are used to calculate the camera extrinsic matrix. Figure 2-6(b) is the mapped image from the calibration showing the raw image points detected on the checkerboard, true world points and calibrated points. It is seen that the calibrated points are very close to the true world points and in the Figure 2-6(b), the mean calibration error is 1.7%. For the calibration shown in Figure 2-7 the mean error is 0.05%. The max deviation from of a calibrated image point is identified and the max error is calculated established by its deviation from the real-world coordinate point.

2.3 Oil droplet shape calibration

The shape assumption of the oil droplet dictates the level of accuracy of the shear stress measurements. Plethora work is conducted in this aspect of study. There are two droplet shape assumptions to be made, the initial shape of the droplet and the shape the droplet acquires during

deformation. Figure 2-1 shows the shape for the droplet under the action of the shear stress and an approximate shape is assumed to simplify the thinning rate calculations. This shape assumption study is also performed in [6] and [14] and have concluded that assuming an obtuse angle triangular pyramid shape (Figure 2-8) yields most accurate results. The other assumptions examined during their study were equilateral triangular prism and right-angle triangular prism.

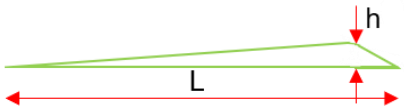

Figure 2-8: Assumed droplet deformed shape.

However, initial shape assumption has studied meticulously in this study. Three initial shapes are assumed: hemispherical (Figure 2-9(a)), Spherical cap (Figure 2-9(b)) and cylindrical cap (Figure 2-9(c)). Given enough time, a silicone oil droplet spreads completely on the surface [15]. But since the droplet is subjected to shear without giving enough time to spread out evenly it is inappropriate to assume a flat profile. Additionally, adding the coloring pigment to the oil slightly alters the pure silicone oil properties and hence it may be inappropriate to assume a complete Newtonian silicone fluid assumption for the oil pigment mixture used.

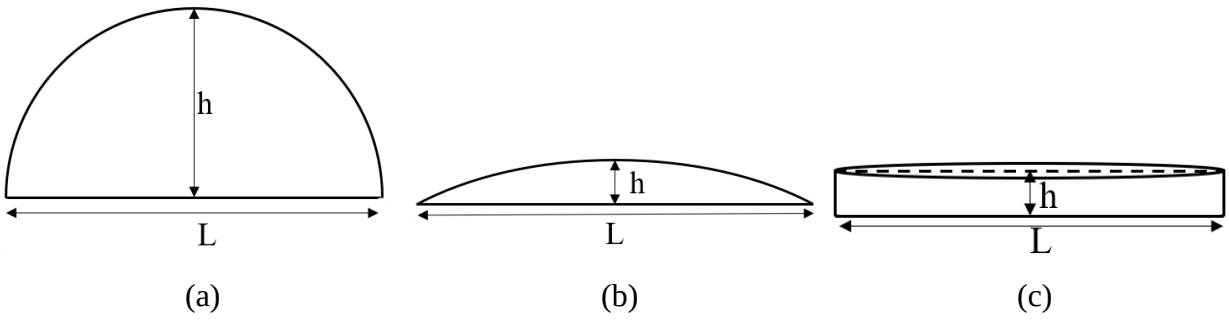

Figure 2-9: Initial droplet shapes considered

A known volume of droplet is pipetted on a surface to verify the appropriate droplet shape assumption. A positive displacement Gilson Microman E M10E, 1-10 μL micropipette is used to accurately dispense the silicon-pigment oil. The pipette has an uncertainty of ±0.09 μL for

dispensing a volume of 1 μL, ±0.1 μL and ±0.15 μL for dispensing a volume of 5 μL and 10 μL respectively. A positive displacement pipette is recommended to use for applications pertaining viscous liquids to avoid the volume dispensing errors due to compressibility effects of air as in general air displacement micropipettes. Figure 2-10(a) illustrates the Gilson micropipette used in this research and Figure 2-10(b) is a zoomed in snipped of the tip showing the piston that is in contact with the pipetting fluid restricting air from entering in between the fluid-piston interaction and thus ensuring the accurate amount of fluid dispensed.

Figure 2-10: (a) Positive displacement micropipette (b) Zoomed in snipped of tip

For the hemispherical assumption made, it is easy to reverify if the assumption holds good by processing the first frame captured. The wetted area by the droplet is calculated from image processing in MATLAB, using which the droplet volume can be calculated. The volume obtained by image reconstruction and the actual volume pipetted out on the plate surface are tabulated in Table 2-1 and it is evident that this assumption is not appropriate as the error in volume calculation

are approximately 1600% to 2000% for 350cst silicone oil and for a higher viscous silicone oil of 1000cst the error reduces to about 1500% to 1700% and hence if using very high viscous oil the hemispherical droplet assumption would be feasible.

Table 2-1: Volume comparison for hemispherical droplet assumption

Oil Kinematic viscosity	Actual	Hemispherical
centistoke	Volume(μl)	Volume(mm^3)
1000	10	182.82
	7.5	167.63
	5	106.39
	1	14.62
350	10	210.94
	5	127.83
	1	16.93

To identify the best assumption of cylindrical and spherical cap shape, one of each droplet assumption data is processed to plot an inverse slope plot with time and seen from Figure 2-11 it is flawless to use the spherical cap assumption as it ensures continuity in the L/h slope during the blowing. Additionally, with the cylindrical droplet assumption, we see that the model has a step increase in the height of the droplet at the start of the blowing which is impractical.

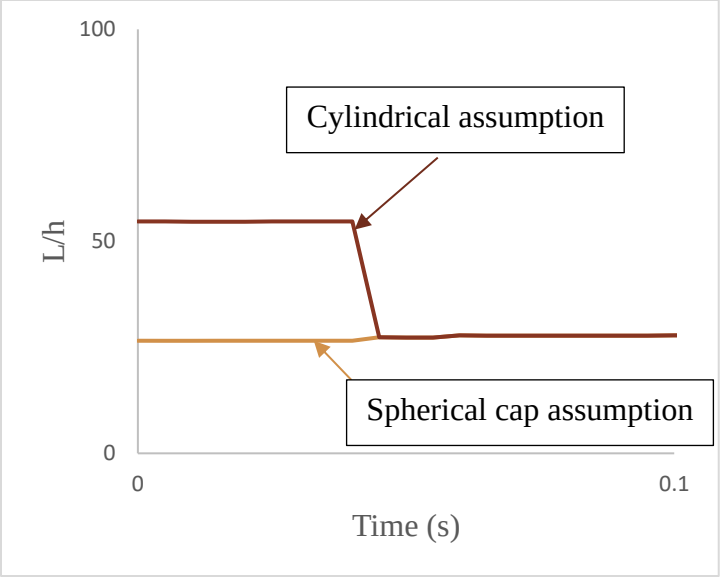

Figure 2-11: Cylindrical and spherical cap assumption comparison

2.4 Oil viscosity calibration

In order to implement the technique discussed, oil dynamic viscosity had to be known accurately to calculate the shear stress. Silicone based oil is used in the experiments in order to reduce the risk of ignition at higher temperatures as in case of petroleum-based oil and to avoid the characterization of oil by high vapor pressure as high-speed testing are associated with low freestream pressure.

An initial kinematic viscosity estimate is provided by the oil supplier. Considerable amount of fluorescence pigment is mixed with the pure silicone oil which is initially colorless. The final oil-pigment mixture helped to pick up the oil droplet precisely with a high-speed camera when illuminated with a UV or blue light. Hence, oil viscosity had to be characterized after mixing it with the coloring pigment. Anton Paar Modular Compact Rheometer (MCR 501) is used to measure the dynamic viscosity of the oil used in the experiments. A concentric cylinder is used to measure the viscosity of the liquid. The cylinder is rotated inside another cylinder which contains the liquid and the force exerted by the liquid on the rotating cylinder to resist the rotational motion is measured and is converted to the shear stress. By repeating this procedure at two different RPM gives two points on a curve which is sufficient to determine the flow characteristics using a suitable model.

The rheometer used is shown in Figure 2-12 which is equipped with an additional fully automatic temperature calibration device which allowed to set the desired temperature and obtain the oil viscosity. The instrument promises error free measurements by utilizing the error free tool master technology which automatically recognizes the geometries and accessories and transfers all the parameters to the software. It also stores the zero-gap position so that the consistency always remains when measuring the viscosity of different oils. Additionally, the temperature controller changes the temperature of the oil when in the sampling adapter and the temperature is displayed from an integrated temperature sensor.

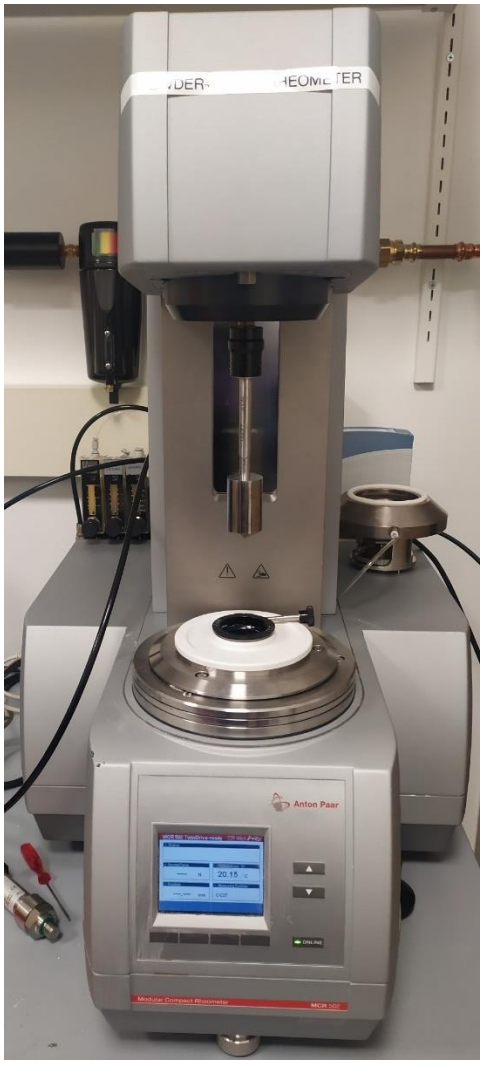

Figure 2-12: Anton Paar MCR502 rheometer

Silicone oil with different viscosity has been used, depending on the expected shear stress and the test duration the viscosity is chosen such that the required oil thinning is obtained before the end of the test and that the viscosity is not too low as to blow away the oil completely. High viscosity is preferred in supersonic testing with a reasonable amount of blow time. For short blowing in orders of a few seconds, less viscous oil must be chosen very carefully such that the droplets thinning with time is achievable.

The viscosity of the final oil obtained was found to change with change in RPM. Particularly, the fluid behaved in a pseudo plastic manner, that is, the viscosity of the oil mixture reduced with increasing the RPM and when the RPM was reduced, the viscosity of the fluid tends to fall back to its initial viscosity. This behavior is demonstrated in Figure 2-13(a) where the viscosity variation tests were performed in a Brookfield DV II pro viscometer also shown in Figure 2-13(b).

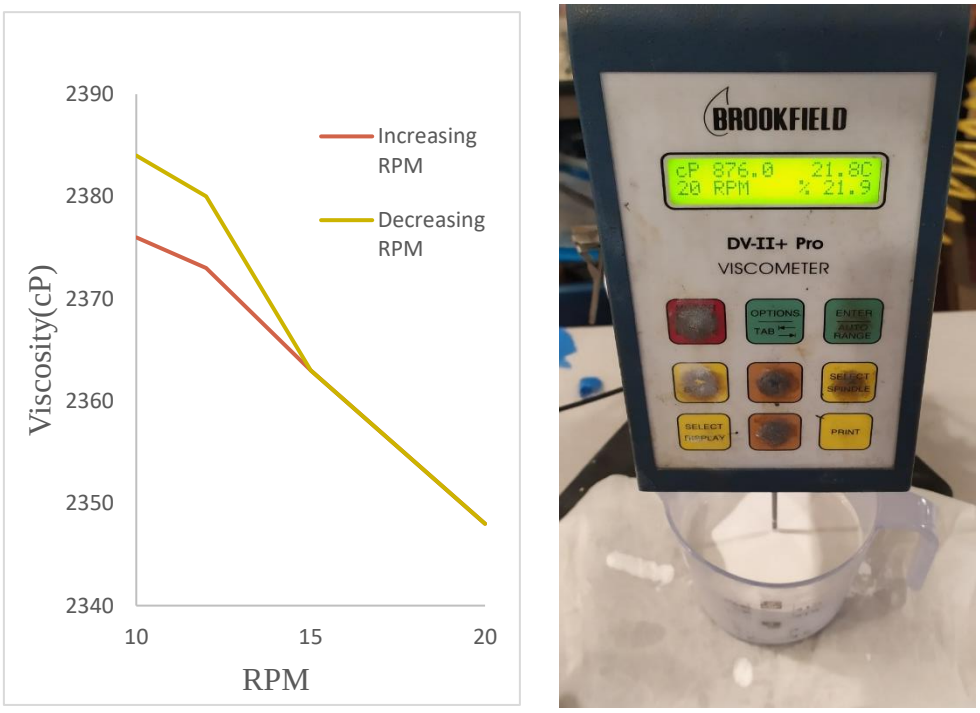

(a) (b)

Figure 2-13: (a) variation in viscosity with RPM (b) Brookfield viscometer used for the test

Now that the oil mixture is no longer Newtonian and the variation of viscosity is observed, it is important to characterize the oil mixture viscosity with the shear rate involved in the tests so that the appropriate level of viscosity is considered for calculations. The velocity of the oil droplet

was calculated with the centered finite difference scheme, with the help of the thinning rate information already available. The shear rate associated was then computed by knowing the local droplet height. These calculations are summarized in Figure 2-14 for the dot evolution of 12500cst silicon oil mixed with TiO_2 pigment. The viscosity of the droplet is disclosed in Figure 2-14(a) and the associated shear rates are disclosed by Figure 2-14(b). It is observed that the shear rate varies from about 0.2 to 3. The variation of viscosity for these range of shear stress was measured by the rheometer and the results are plotted in Figure 2-14(c). The variation of in the level of viscosity is about 0.9%, which is considerably low and must not affect the shear stress calculations and hence this effect can be ignored. Moreover, when considering lower viscous liquids, the shear rate tends to fluctuate significantly, however, the viscosity variation was calculated to still remain <2%. Based of this analysis it is preferred to go with higher viscous oil whenever possible to reduce the inaccuracies in the shear stress calculations.

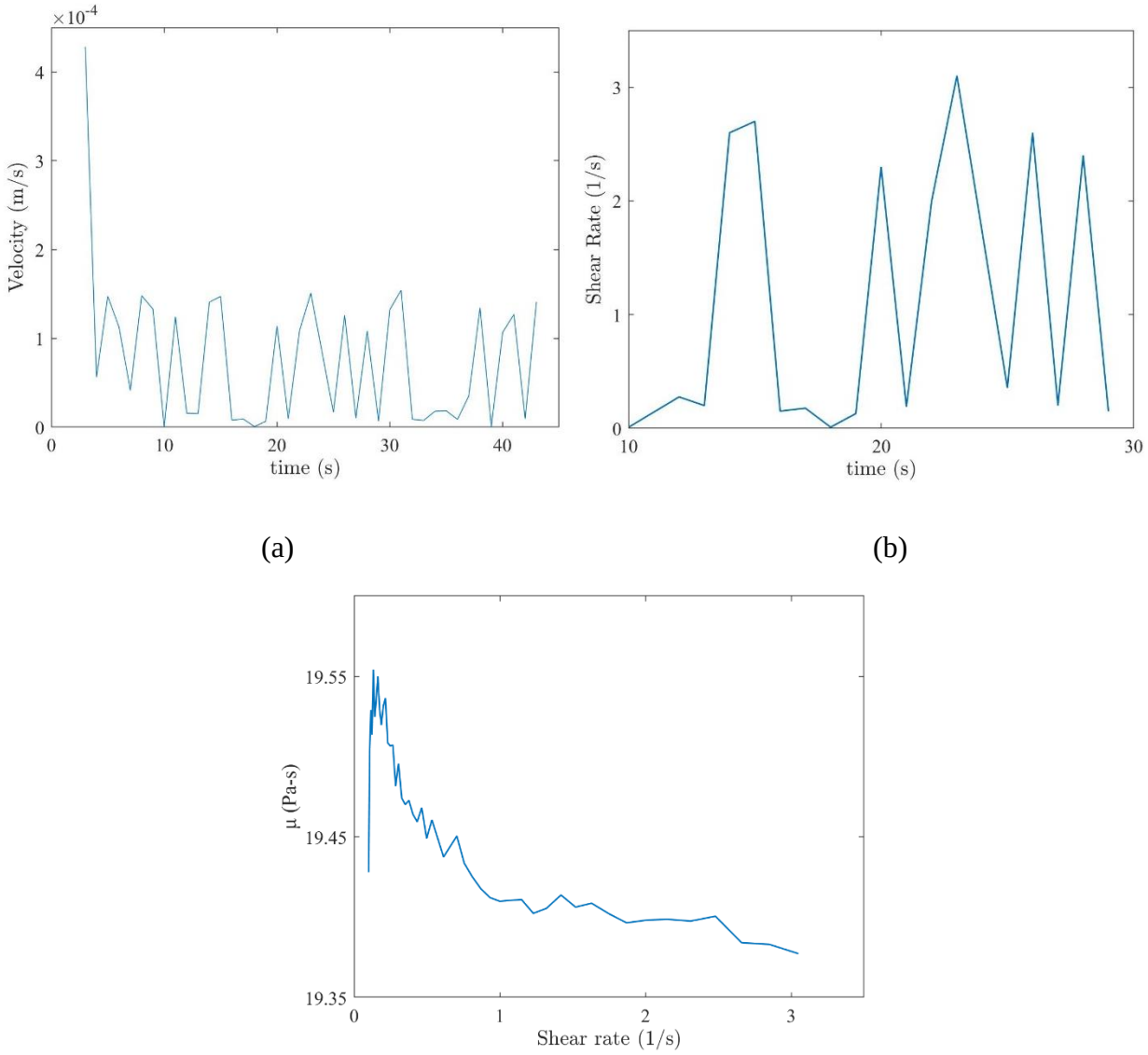

Figure 2-14: Viscosity calibration with shear rate

Finally, the oil mixture is also calibrated with temperature as the well-known trend is expected and achieved in Figure 2-15. The viscosity of the oil reduces with temperature and hence it is important to note the test static temperature to be able to use the appropriate oil mixture viscosity for the test performed. The oil calibration test was also performed in the rheometer equipment shown in Figure 2-12. The temperature add-in available with the instrument makes the temperature variation tests much simpler and since the oil or the instrument itself is left undisturbed; the error free calibration is obtained.

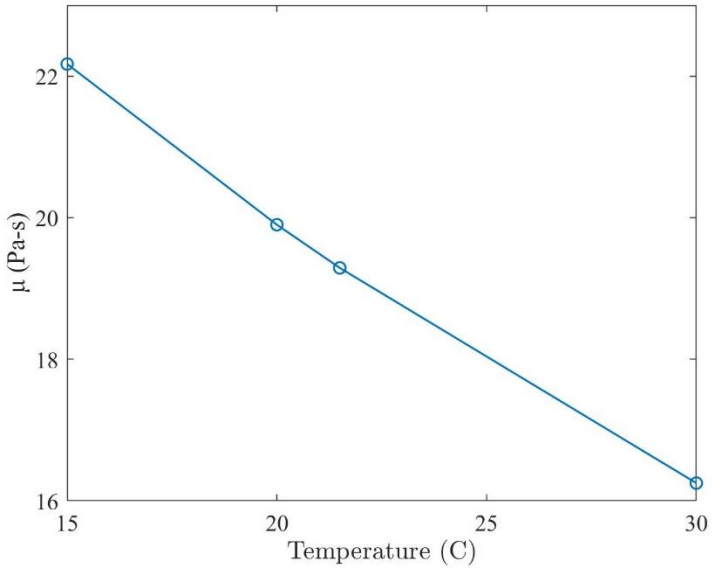

Figure 2-15: Variation of viscosity with temperature

2.5 Image/video processing

Oil droplets deposited on the model are tracked with a high-speed camera and image construction is implemented to accurately calculate the wetted area and estimate the height of the oil droplet. Each of the frame captured during the test is calibrated with the camera calibration matrix to remove any distortion errors due to lens. This process is consistent for all the tests performed and is used in conjunction to obtain the flow viz around complex models by applying matrix of small oil droplets and tracking each of the droplet with time, the formation of secondary flows is well captured and the plotting the streak lines would help in determining the real-world dimensions of secondary flows.

It is important to confirm certain aspects before performing the experiment, such that the height of the droplet is in the range of satisfying the lubrication theory, the oil pigment mixture is Newtonian/ Pseudo Newtonian, the droplet is sufficiently large to occupy certain pixels in the image and is well illuminated with respect to the background to be picked up by the camera.

During each test series or matrix of small oil droplets have deposited on the surface to be studied. The matrix of droplets helps us to obtain the evolution of secondary flows and as the frames are recorded in real time the formation structure of secondary flows is evident.

Post processing is done using MATLAB routine, consisting of first subtracting the background image (Figure 2-16(b)) from each raw frame (Figure 2-16(a)) thereby discarding

major noise from the image and then undistorting the image for any lens distortion using a camera calibration coefficients generated with multiple calibration images. So far the image is an indexed image that is, it is a 3D (image X 3) matrix where each matrix in third dimension is associated with the color map red, green and blue. Now, the indexed grayscale image is passed through a certain threshold filter to accurately capture the shape of the oil droplet. Figure 2-16(c) is the subtracted, threshold - calibrated image obtained. Next, the boundaries of each of the droplet is identified as demonstrated by Figure 2-16(d). For the shear stress computation, the thinning rate or the slope of the droplet is required for which height information has been calculated which is derived using the wetted area of the droplet and shape assumption as discussed in section 262.3. A ROI mask is employed for shear stress computations as only a few droplets are considered to calculate the shear stress and the rest of the region can be ignored; however, this is not possible for flow visualization as the ROI surface for flow visualization is mostly spread over the entire frame. Further, a gradient mask of the image is obtained in order to amplify the detected droplet boundaries which is then filled with the glowing pixels to hide any holes and finally the shape of the droplet is accurately traced. The process of dilating the image helps in overcoming some of the background glowing pixels (noise) generated during threshold filter. The final image therefore obtained by processing the image to reduce noise is shown in Figure 2-16(e). From this image, boundaries are traced out where there is a change in glowing pixel. Figure 2-16(f) shows the image overlaid with the boundaries traced by the MATLAB routine. As observed, there is some noise in the image at the trailing edge of the turbine blade which is interacting with the last row of the droplets and therefore the detailed information at those droplets is mostly lost.

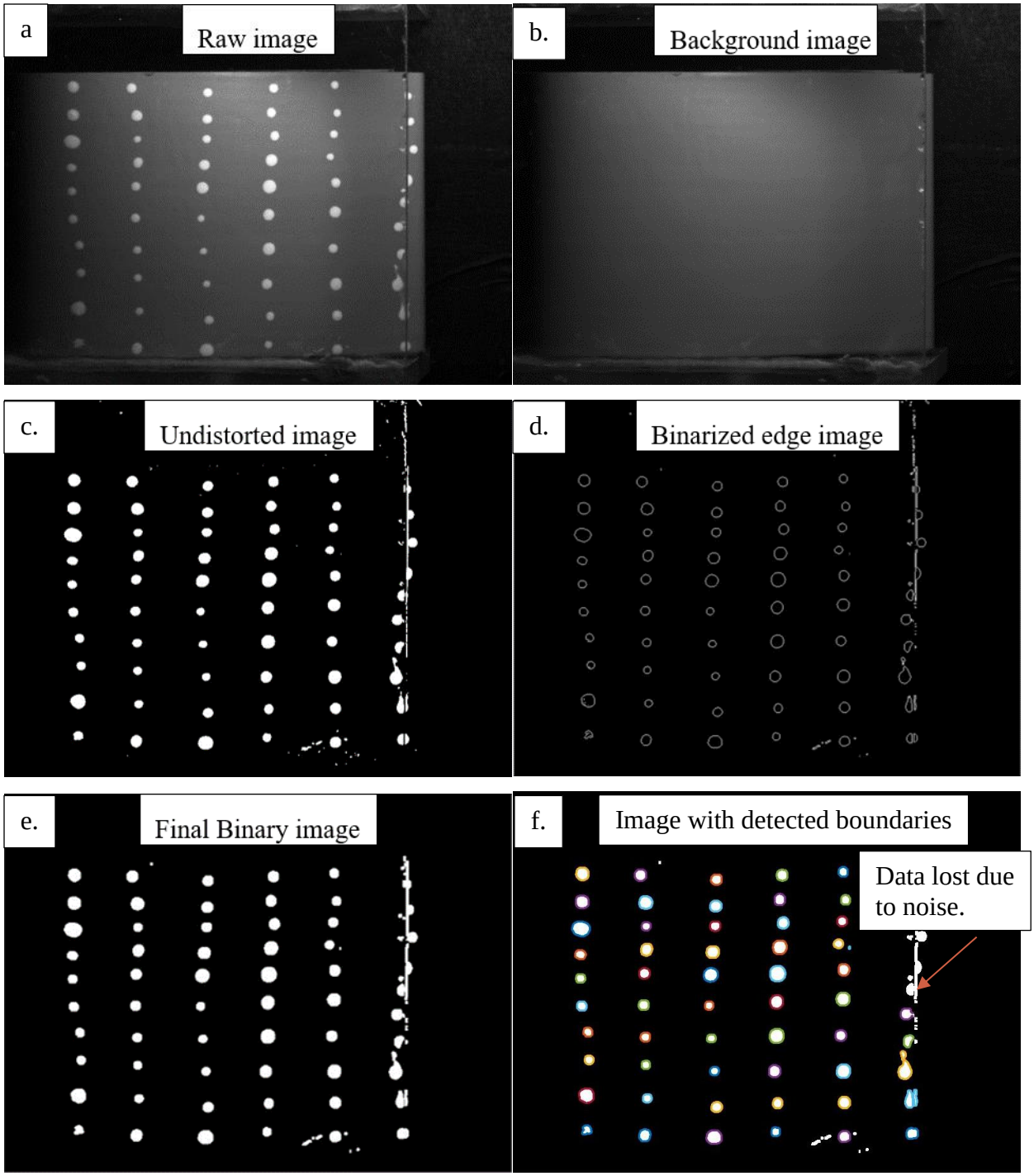

Figure 2-16: Image processing module

Now that the boundaries of the droplet are accurately captured, the next step is to map the boundaries to the real-world coordinates using the camera parameters calculated with calibration image, the wetted area as well the length of the droplet can be obtained in millimeters. From the

obtained wetted area and droplet shape assumption, slope of the droplet is calculated and therefore, the shear stress is obtained. Figure 2-17 is the mapped image obtained using the detected boundaries shown in Figure 2-16 (f).

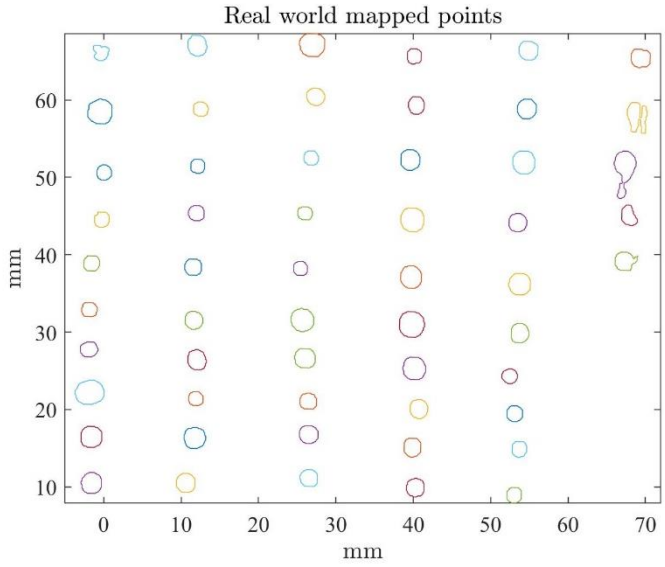

Figure 2-17: Mapped image

This routine is applied to each frame when processing the images captured from a camera. Alternatively, image masking is employed if tracking a specific droplet, image masking generates all zeros in the entire frame, but the ROI selected in the frame. Hence, this is an efficient way for reducing all the background noise and only having the required droplet in the ROI mask. The downside of this approach is that it only tracks the droplets in the ROI may have to run the routine several times to capture the thinning rate for multiple droplets.

Processing a video follows a similar approach, however, it tracks the same points throughout the video instead of defining new set of points for each frame as in case of image processing. The video processing solver picks up undistorted frames from the video and detects the boundaries in the last frame of the video. This approach is chosen as the oil droplet is deformed at the last frame and max number of points can be defined at this frame. The MATLAB routine asks if the user want to track the evolution of that particular droplet, this seems to be a reasonable approach as sometimes the MATLAB also detects some of the background pixels if sufficiently large as droplets and this step helps the user to just skip to track if any noise picked up by the code. Once this step is done the points detected are fixed and the same points are tracked with time

throughout the video with the video playing back in time. The video used for tracking is generated with the undistorted frames implying that the video does not follow the same processing as the image processing. The points are tracked in a grayscale video whereas the frame boundaries are tracked in a binary image. The video processing and tracking solver requires the video to be in the grayscale format and the points are tracked based on the color gradient and bidirectional error across the droplet boundaries.

Now that two different processing routines are developed and used it is important to understand the difference associated in processing solvers developed. Figure 2-18 summarizes the variations obtained by processing the data for the same oil droplet using frame processing and comparing the data obtained by tracking the same droplet using the video processing solver. It is observed that there is a significant change in the slope variation of about 6.7% which will not considerably affect the calculated shear stress. It is challenging to comment one if this solver is the best over other, based on the quality of images captured during the test, the results obtained by one solver may be prevalent than another.

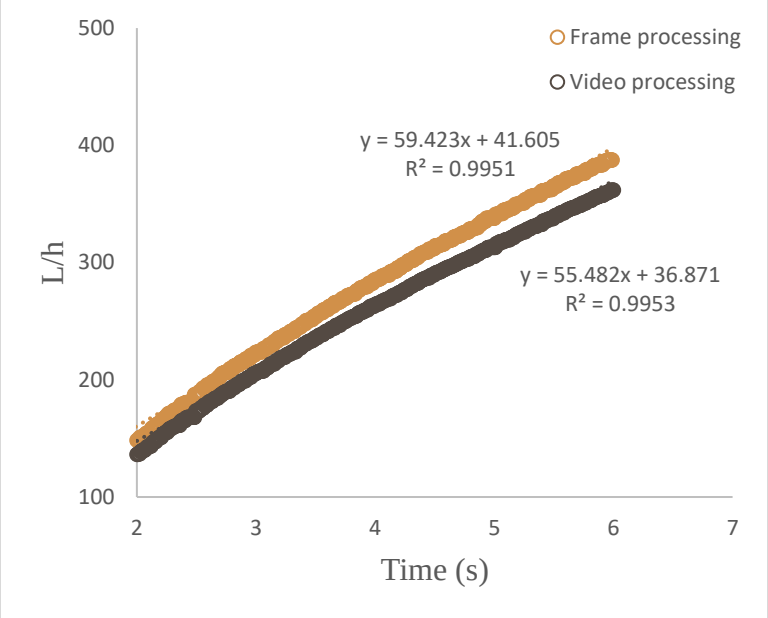

Figure 2-18: Variation in different processing solver

2.6 Methodology for Streak lines plotting

The novel part of this research is merging two measurement techniques, this gives the advantage of procuring the data required for both of the measurements in a single run, providing flexibility to implement other measurement techniques simultaneously which helps in getting the test done sooner without the need for repeating the experiments, data processing for both of the techniques can also be clubbed to an extend therefore reducing the computational cost of processing the data independently.

Captured video is used as a base input to observe the flow behavior around any complex objects and identify the flow structures and flow direction around the objects, finally, a streak line plot is obtained demonstrating the overall flow field over the surface. As illustrated in Figure 2-19, the captured video also helps in identifying the direction of skin friction by the effects of wrinkles formed during the initial deformation of the oil droplet.

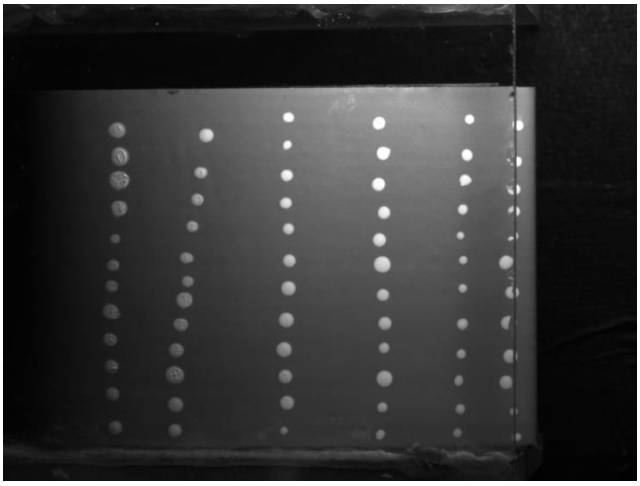

Figure 2-19: Raw frame during the start of blowing

The methodology remains the same as mentioned in shear stress measurement section (2.5) as the same oil dots are used to get the flow visualization data as well. However, mush intense information such as oil viscosity, droplet thinning rate are not required to plot the streak lines. Streak line plots are obtained by pretty much following the same approach as discussed in section 2.5. Once the boundaries are obtained from Figure 2-20(a), the skeleton of the oil droplets is obtained as in Figure 2-20(b). That is the pixels along the oil droplets are shrunk until a fine oil droplet skeleton is obtained. With the shrunk oil droplets obtained it is now easier to plot the streak

lines by combining the aligning streak lines and identifying the separation regions where the oil droplet has not been moved. If the volume of the droplets applied are consistent then based on the distance travelled by each droplet it is possible to estimate the regions of higher and lower shear stress. Lastly, as the frames are captured in real time, it is possible to identify the flow direction, vortex formation direction and with the mapping the real-world dimensions of the secondary flow structures formed can be found along with the position of the flow structures.

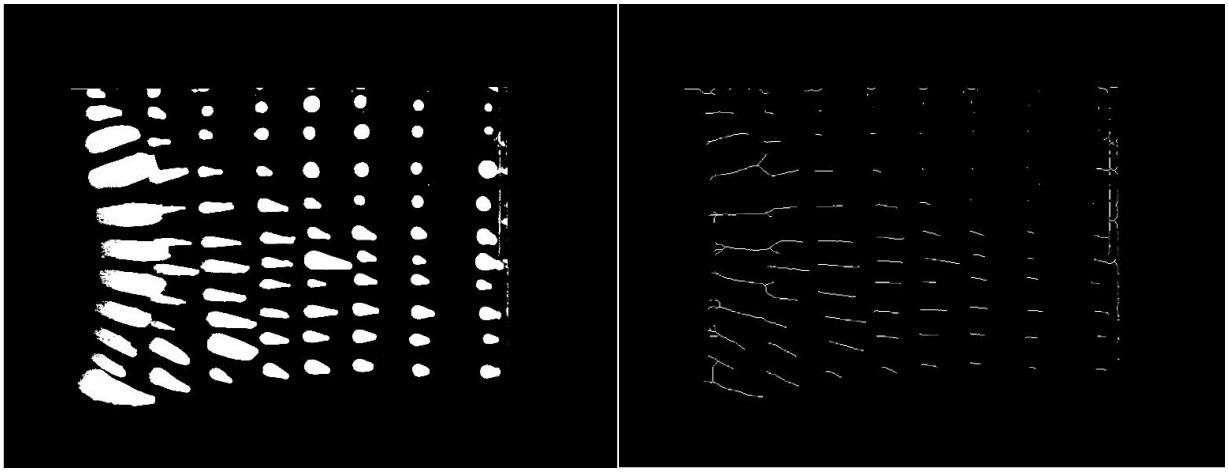

(a) (b)

Figure 2-20: Streak line plotting methodology

2.7 Uncertainty quantification

The uncertainty in the shear stress calculated is determined by the individual uncertainty involved in each if the parameter involved in calculating the shear stress. The MATLAB routine calculates the thinning rate of the droplet based on the image acquisition and processing quality and the volume of the droplet. The final shear stress calculations are dependent on the uncertainty in the slope of the thinning rate of the deformed droplet and the viscosity of the oil used. Therefore, the parameters affecting the uncertainty in the shear stress measurements can be summarized in the tables below. In order to calculate the sensitivity of each of the parameter to shear stress, the shear stress is calculated by adding the uncertainty value to each of the parameter and inspecting the percentage change in the shear stress values. To calculate the total uncertainty in the shear stress, [16] is employed. Here the root mean square error for each of the quantity is accounted for to the total uncertainty in the shear stress calculations.

Table 2-2: Uncertainty table for low viscous oil

	Value	Units	Uncertainty	Sensitivity to Shear stress (%)
Volume	1	μL	0.09	8.2
Temperature	22	C	12	17
Droplet length	4.318	Pixel/mm	1	4.9
Slope	50.34		0.15	0.3
Shear rate	0.3	s^{-1}	15	0.4
Shear stress	91.62	N/m^2	Total Uncertainty	8

Table 2-1 provides a detailed summary on the uncertainty estimation employed in the study. The uncertainty in Volume is obtained from the micropipette used to dispense oil on the surface of the model. The rheometer offers uncertainty free measurements or the uncertainty in viscosity measurements is 0.0001Pa-s which is too low to be considered for uncertainty analysis. A temperature is value is used when calculating the shear stress of using the oil droplet, but the temperature of the flow varies during the test. Figure 2-21 shows the variation of temperature during the test, an approximate of 12˚C variation is observed and is used as the estimate uncertainty for the uncertainty analysis. Based on the resolution of the frames acquired and the FOV, the real-world coordinate size of the frame is calculated, followed by the pixel per unit length calculations and an uncertainty of 1 pixel is assumed to perform the uncertainty calculation. From the tinning rate obtained from the code, the slope was calculated and the associated error in the slope was obtained for uncertainty quantification. As discussed earlier, the variation in shear rate does not significantly affect the shear stress calculations. In the calculations above, the entire variation spectrum of shear rate is considered to perform the uncertainty over the entire domain.

As can be concluded from the uncertainty analysis, the shear stress calculations are most sensitive to the droplet volume and droplet temperature and least sensitive to shear rate variations. Hence, it is very important to carefully dispense the oil without including human errors and by using the local temperature of the during the time of deformation, the temperature uncertainty can b=be reduced. An effective MATLAB routine should be implemented to accurately capture the droplet boundaries to avoid any associated pixel errors. Slope have marginal uncertainty towards

the shear stress calculations and overall a total uncertainty of 8% is expected in shear stress calculations.

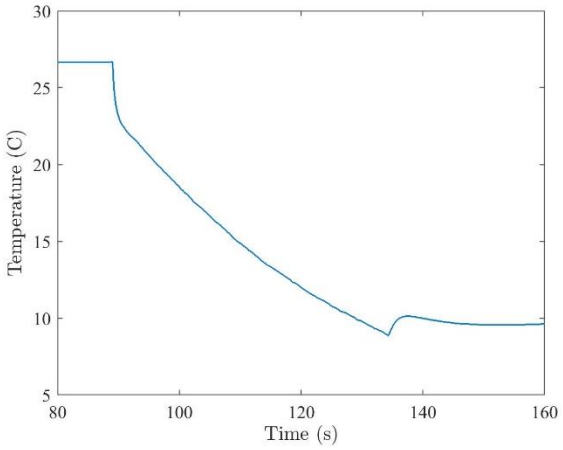

Figure 2-21: Temperature variation in SACOC testing

There is however another parameter to consider. Discussed earlier are two MATLAB routines developed to track the droplets and calculate the thinning rate, the processing of frames and video. It is expected that both these routines provide the same results as they are tracking the same droplet, but the results obtained from both of these routines differ by about 10%.

Frames are used to process to data as they are much accessible when compared to the video where the points are tracked using an algorithm. Another drawback of using video processing is the vibrations involved in testing. During data acquisition there are certain vibrations picked up by the camera and since video processing depends on the information from the preceding frame, the vibration tends to shift the entire frame and some of the point struggle to stay on the boundaries and fall into the droplet. An example is shown in Figure 2-22 where (a) is the first video frame processed at t=n, this approach helps in defining a greater number of points along the edges of the droplet to be tracked. And Figure 2-22 (b) is the last frame tracked by the code at t=0, as observed the boundary of the droplet in the frame is not accurately captured.

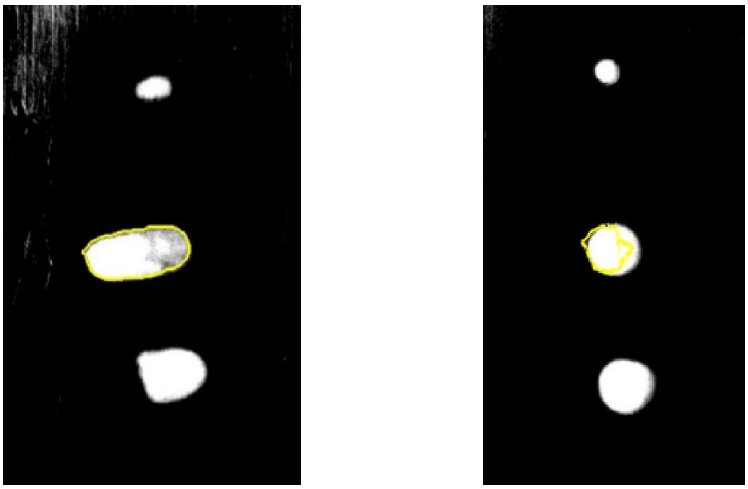

(a) (b)

Figure 2-22: Video processing routine (a) First frame (t=n) (b) Last frame (t=0)

Table 2-3 provides an uncertainty quantification for a high viscous oil. The same approach is used, and a similar uncertainty value is obtained.

Table 2-3: Uncertainty table for high viscous oil

	Value	Units	Uncertainty	Sensitivity to Shear stress (%)
Volume	1	μL	0.09	8
Temperature	22	C	12	23.9
Droplet length	4.318	Pixel/mm	1	15.6
Slope	2.75		0.06	2.2
Shear rate	0.3	s^{-1}	2.7	1.5
Shear stress	53.05	N/m^2	Total Uncertainty	7.1

3. EXPERIMENTAL CAMPAIGN

In an effort to prove the applicability of the developed measurement technique, several tests have been performed and the results are compared with the empirical/CFD results to attain a level of satisfaction about the developed measurement technique.

3.1 Flow over a Flat plate

A Simple flow over a flat plate was considered to validate the developed measurement technique. The abundant literature and analytical solutions available for the flow over a flat plate at various flow conditions makes it an ideal choice to consider for validation purposes.

A sharp leading edge flat plate is used for validation. Several droplets are applied at a known location on the surface of the flat plate and are tracked with a high-speed camera. Blasius solution is used to compare the experimentally calculated shear stress to the empirical solution.

3.1.1 Experimental set-up

The testing was carried out in a wind tunnel at arms lab at Purdue University. The wind tunnel had a test section of *3 ft X 6 ft* with complete optical access which facilitated using the camera and light source. The flat plate of *1ft X ½ ft* was machined to have a sharp leading edge, making it compatible to use the Blasius solution for validation.

The frames are acquired at 16Hz as this is a low-speed testing, the oil droplet takes longer time to deform. A positive displacement Gilson micropipette shown in Figure 2-10 is used to accurately dispense the required amount of oil on the surface of the model. Two 1μl, two 2 μl, one 3μl and one 5μl are applied at 0.1 *m* downstream of the plate.

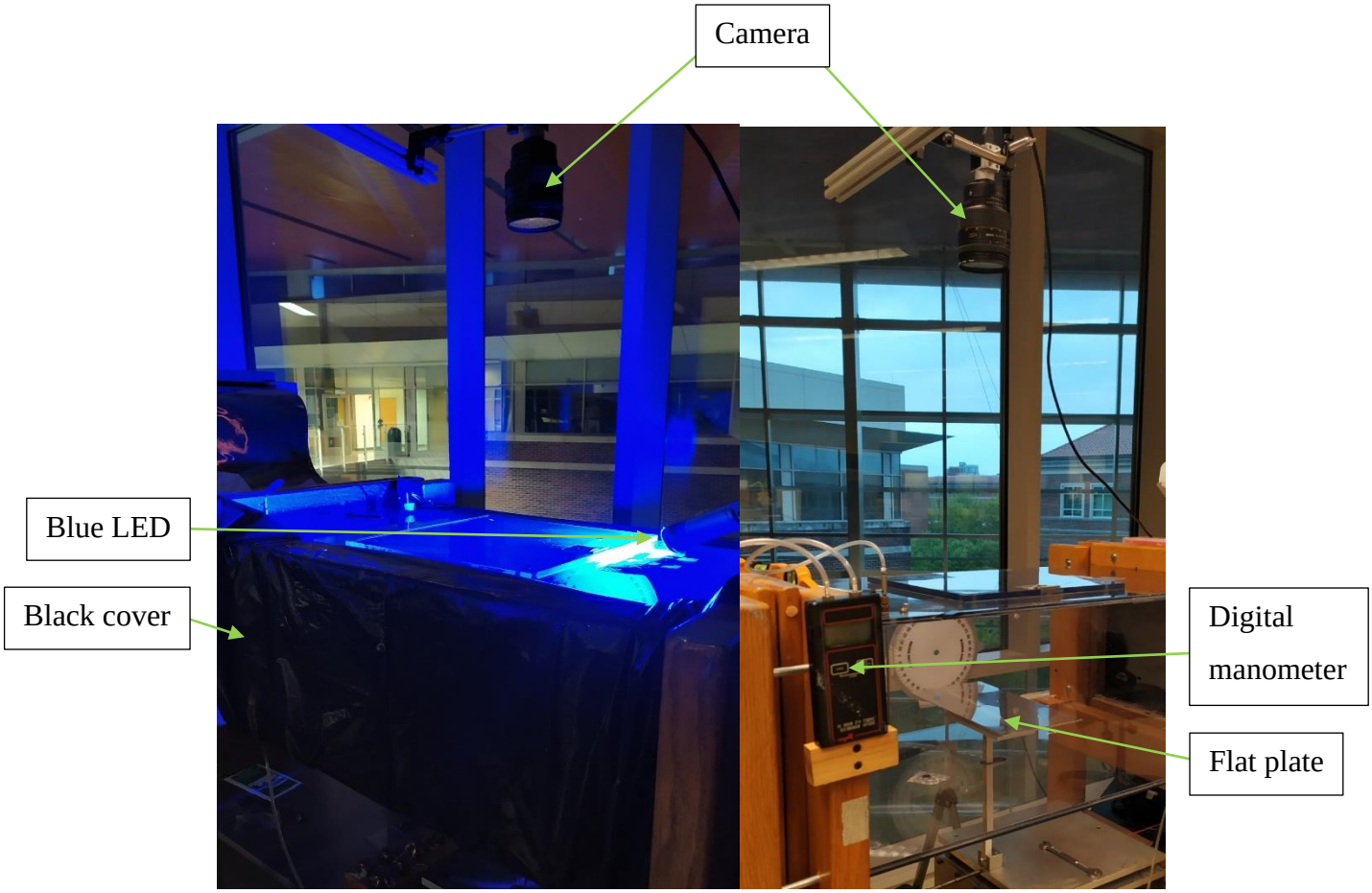

Figure 3-1 Experimental setup for Flat plate

The test was conducted at low subsonic conditions with the freestream velocity of 19.8m/s corresponding to Reynold number per unit length of $1.277*10^6$ m^{-1}. Figure 3-1 shows the experimental setup. An acA800-510um Basler ace camera is used to record the frames and a blue LED is used to illuminate the oil. The camera has a maximum acquisition frame rate of 511fps with a resolution of 800 X 600 pixels. TiO_2 pigment has a property to illuminate under UV light and blue light is readily available comprising the closest wavelength to UV spectrum of 410nm - 455nm, where the wavelength of UV spectrum is just less than 400nm. A black plastic sheet is used to cover the optical access to the test section from the sides in order to restrict any visible light entering the test section from the sides. A digital manometer is used to obtain the differential pressure and calculate the corresponding free stream velocity.

3.1.2 Results

First off it is important to double check if the thickness of the droplet is small enough to remain in the boundary layer developed on the flat plate. To compare the height of the droplet with the boundary layer thickness over a flat plate the equations 3. 1 and 3. 2 are used.

$$\delta_{\text{laminar}} = 5\left(\frac{\nu x}{U}\right)^{1/2} \quad 3.\ 1$$

$$\delta_{\text{turbulent}} = 0.37 x Re_x^{-1/5} \quad 3.\ 2$$

Figure 3-2 demonstrates the boundary layer profile obtained by equation 3. 1 and 3. 2, where equation 3. 1 and 3. 2 are boundary layer profile for laminar and turbulent air flow obtained from Blasius solution and 1/7th power law, respectively. The markers on the plot are the experimental data obtained for height evolution of the oil droplet for different droplet volumes. It is observed from the plot that the height of the droplet remains in the laminar boundary regime at all length for all drop volumes dispensed on the flat plate. It is expected to have the droplet height evolution in the laminar regime as the test was conducted in a low subsonic wind tunnel with air inlet from the surroundings without any compressible effects.

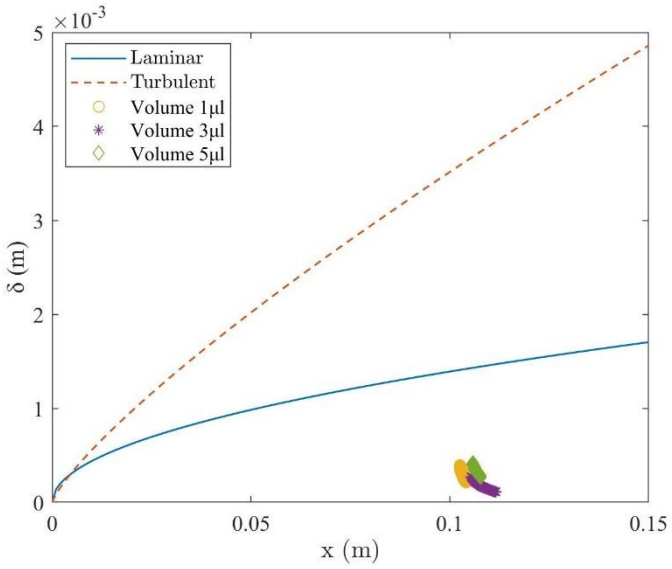

Figure 3-2: Boundary layer thickness comparison with height evolution of droplet

Inverse of slope variation of two droplets on the plate are shown in Figure 3-3. The time window considered for studying the thinning rate based on the requirement of the linear variation of the inverse of slope with time such that the slope of the line acquired by this technique helps in calculation of shear stress at that particular location. The time window considered in Figure 3-3 is 20s to 24s and the R^2 obtained is close to unity, this is obtained at the cost of less experimental data, excluding the points the linear fit contours are not high.

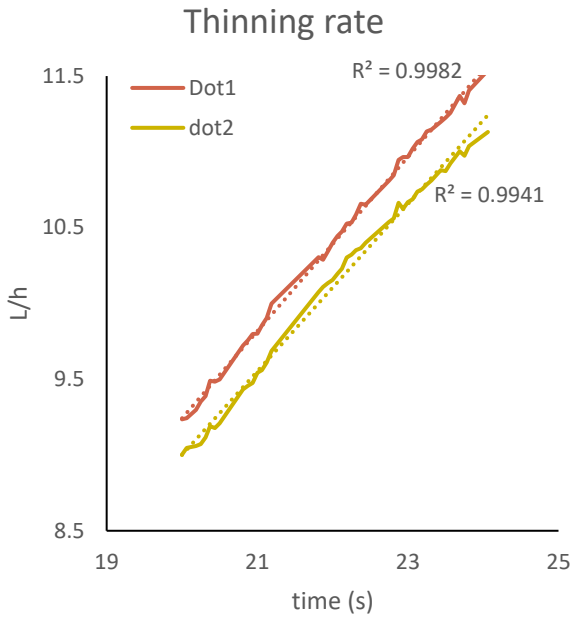

Figure 3-3: Thinning rate variation of droplets on the plate

The experimental shear stress can now be calculate using the equation 2. 15. The experimental shear stress is compared with the empirical shear stress obtained by equations 3. 3 - 3. 6. Equation 3. 3 is the Blasius equation for shear stress distribution over a flat plate for laminar flow and equation 3. 4 is the $1/7^{th}$ power law for shear stress distribution over flat plate for turbulent flows and the equations 3. 5 and 3. 6 are considered to account for any compressible effects in the experiment, where each of these equations represent the shear stress distribution over flat plate in a laminar and turbulent flow, respectively.

$$\tau = \frac{0.332\rho U^2}{Re_x^{1/2}} \qquad 3.\ 3$$

$$\tau = \frac{0.029\rho U^2}{Re_x^{1/5}} \qquad 3.\ 4$$

$$\tau = \frac{1}{2}\rho U^2 0.664 Re_x^{-1/2}\left(\frac{1}{1+0.1296M^2}\right)^{0.65} \qquad 3.\ 5$$

$$\tau = \frac{1}{2}\rho U^2 0.079 Re_x^{-1/4}\left(\frac{1}{1+0.1296M^2}\right)^{0.65} \qquad 3.\ 6$$

The results obtained from the above-mentioned equations are plotted in Figure 3-4. It is observed that there are no compressible effects in the test as mentioned earlier. The experimental data is denoted with the marker and is seen to be in within the 95% confidence level of the shear stress calculated using Blasius solution. As expected, the experimental data matches closely with the laminar shear stress distribution for flat plate calculated by equation 3. 3. The experiment was conducted at very low subsonic speeds and hence a low viscous oil was used to obtain the thinning rate, this could be a reason for the slight deviation of the results from the theoretical calculations. As discussed in the viscosity calibration section of the report, the viscosity of the oil varies significantly for low viscous oils.

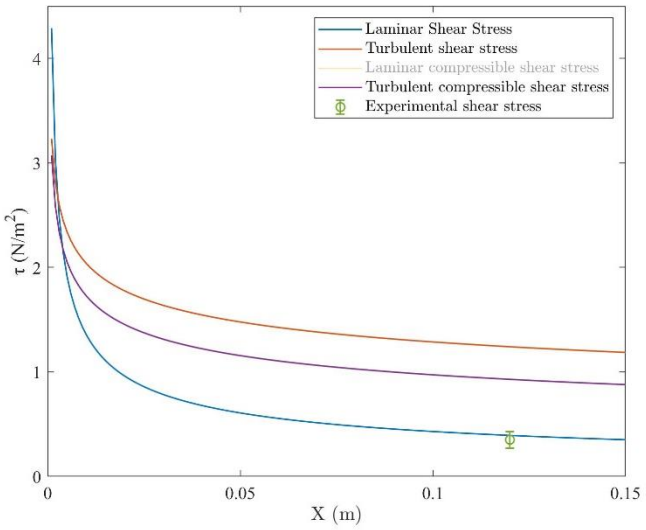

Figure 3-4: Shear stress comparison for flat plate

3.2 Flow over heat exchanger fins

This test was performed on a heat exchanger SACOC (Surface Air Cooled Oil Cooler) fins and study the impact of the heat exchanger fins on the aerodynamics of the secondary flows. One of the applications of SACOC is in the gas turbine engines to use the SACOC heat exchanger model to cool the oil circuit in the gas turbine using the bleed air. As most of the thrust in a gas turbine engine is generated from the bypass air, it is crucial to investigate any aerodynamic losses occurring due to the presence of fins in the bypass duct.

Oil technique is used to calculate the shear stress acting on the fins as well as flow visualization post processing module has been implemented in this campaign to investigate the secondary flows occurring in the heat exchanger fins. The obtained experimental results are validated with the CFD results.

3.2.1 Experimental set-up

The experiment was performed in LEAF (Linear Experimental Aerothermal Facility) test section of the PETAL (Purdue Experimental Turbine Aerothermal Laboratory) tunnel at Zucrow labs, Purdue University. The experimental facility comprises of compressor tanks delivering compressed air with a preset mass flow to the test section which is then ejected into the vacuum

tank. The facility can achieve a Reynolds number in rang of $0.6X10^5 – 2.7X10^6$ with Mach ranging from 0.1 to 6.0.

The SACOC experiment performed in LEAF is split into capturing the two parts, capturing the flow dynamics on the heat exchanger fins, and capturing the flow structure in between the fins.

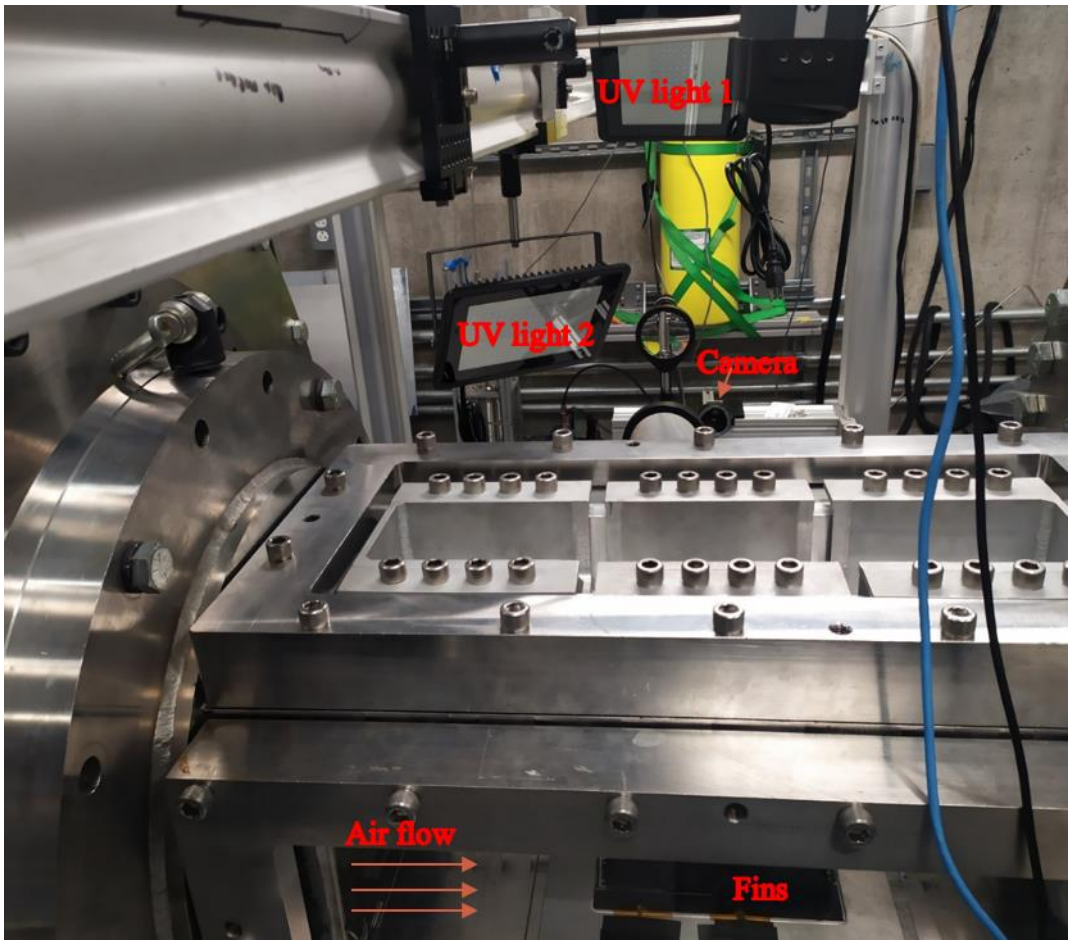

Figure 3-5: Experimental setup for flow over fins captured from side

Figure 3-5 demonstrates the experimental setup for the flow captured on the surface of the fins. The fins are mounted on the LEAF test section and the flow direction is from left to right, flowing at Mach 0.3. The total temperature of the flow is 265K and local static temperature of the plate 283K- 295K . For this test two UV lights were used represented as UV light 1 and UV light 2 in Figure 3-5.

Silicone oil mixed with different UV coloring pigments bought from risk reactors were used for this testing. The oil droplet pattern applied on the surface of the fins is shown in Figure.

Two different colors are used to identify the secondary flows and the droplets are concentrated at the leading and trailing edge of the fin to correctly capture any leading and trailing edge vortices.

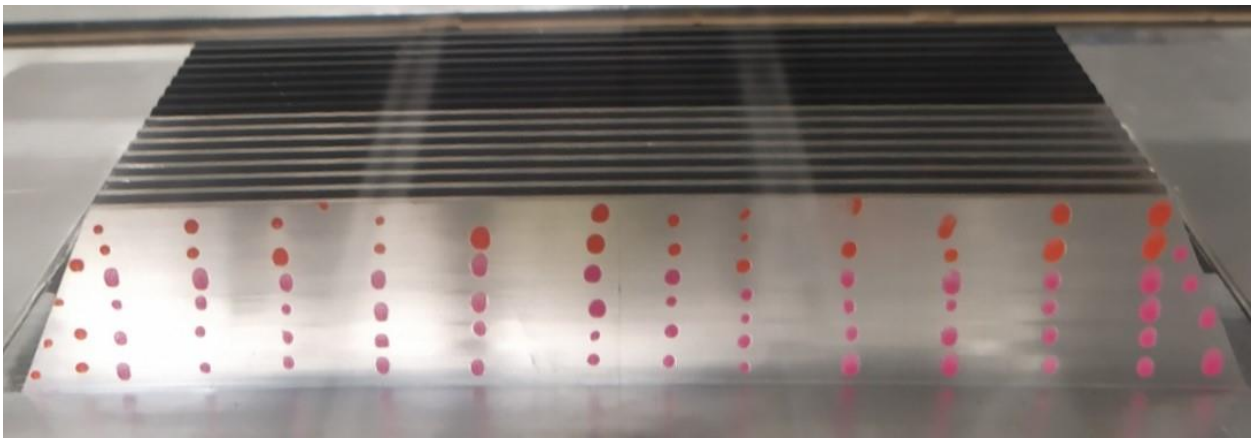

Figure 3-6: SACOC model with oil droplet pattern on one side of the fin

The second setup used to capture the secondary flow structure in between the fins is displayed in Figure 3-7. During this test two different test conditions were targeting by applying two different viscosity oils on the plate to capture flow structure and calculate the shear stress the test conditions involved during the test are a Mach of 0.5 with a total temperature of 264.8K and the local plate temperature ranging from 283K to 295K. The second test conditions include the Mach of 0.3 with a total and local wall static temperature of 265K and 283K- 295K. During these tests, a blue LED was used for illumination. Although the UV light provided better droplet illumination, there were fluctuations from the UV light captured by the camera which altered the droplet area by generating pulsating glowing in the droplet border pixels.

Here an effort is made to apply oil in between the fins in order to validate the separation and reattachment region occurring in between the fins and a row of oil droplets are applied just upstream the fins and a final row of oil droplets 30mm upstream of the oil were placed to aid in shear stress calculations.

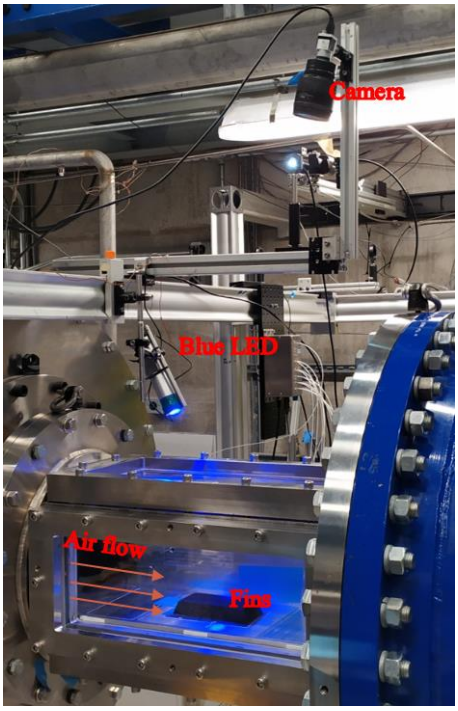

Figure 3-7: Experimental setup to capture flow structure between fins

3.2.2 Results

Results obtained on the side of the fins are discussed first followed by the results for the flow captured from the top of the fins. For the flow over the fin from the side view, the flow evolution with time is described in Figure 3-9.

The flow is from left to right side of the page and as observed from the droplet evolution, at t=3.5 *s* we can see the development of the flow and at the leading edge, the droplets try to split at certain regions showing the presence of secondary flows at the corner regions. At a later time of say t=20 *s*, the developed flow structures are seen, upon carefully studying the droplet evolution at each time, the direction of the flow can be noted. And it is seen that at the leading edge there exists a separation point at the top edge of the fin, as the droplet at the top edge remains stationary throughout the time indicating the stagnation point and droplet next to it moving in the upstream direction indicate the presence of the recirculation region just below the stagnation droplet.

Moving to the lower region of the leading edge of the fin, it is clearly seen that the oil droplet at the lower end bisects, and one streak follows the leading-edge slope of the fin whereas the other streak is deflected downwards. The oil in the second row downstream to the fin travels upward showing the presence of a recirculation region generated form the lower end flow as well

and droplets in the second row applied are distinct as shown in Figure 3-6, but at the final time we see that the droplets have merged into a straight line. Except for the lower two droplets in this row, all other droplets are deflected upward and try to flow in the upstream direction. This effect is due to the leading-edge shape of the fin, where at the lower end of fin, the flow enters the fin, but the region above still has a lower pressure region due to slope of the fin and hence the flow is deflected towards the edge of the fin forming a vortex structure at the leading edge of the fin. This movement of the flow in the leading edge can be understood better by watching the video of the flow evolved at the leading edge also attached in the appendix section of this report.

Apart from the interesting phenomenon occurring at the leading edge of the fin, the flow appears to be attached to the surface at all times and flow in a straight laminar fashion, except at the top end of the fin where the flow is directed upward which makes sense as the flow is trying to overcome the pressure gradient created due to the fin. The trailing edge oil droplets are found to turn around the fin side surface and extend to the behind surface of the fins.

A streak lines plot is traced out of the final frame captured from the test and is mapped to the real-world units to quantitatively decipher the exact locations of the recirculation, separation and deflection regions occurring on the surface of the fins. The streak line plot is shown in Figure 3-8.

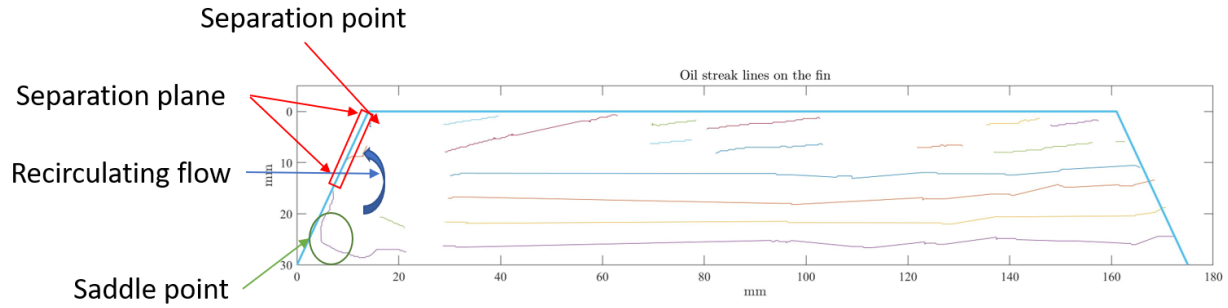

Figure 3-8: Streak lines plotted on the fin surface from experimental data

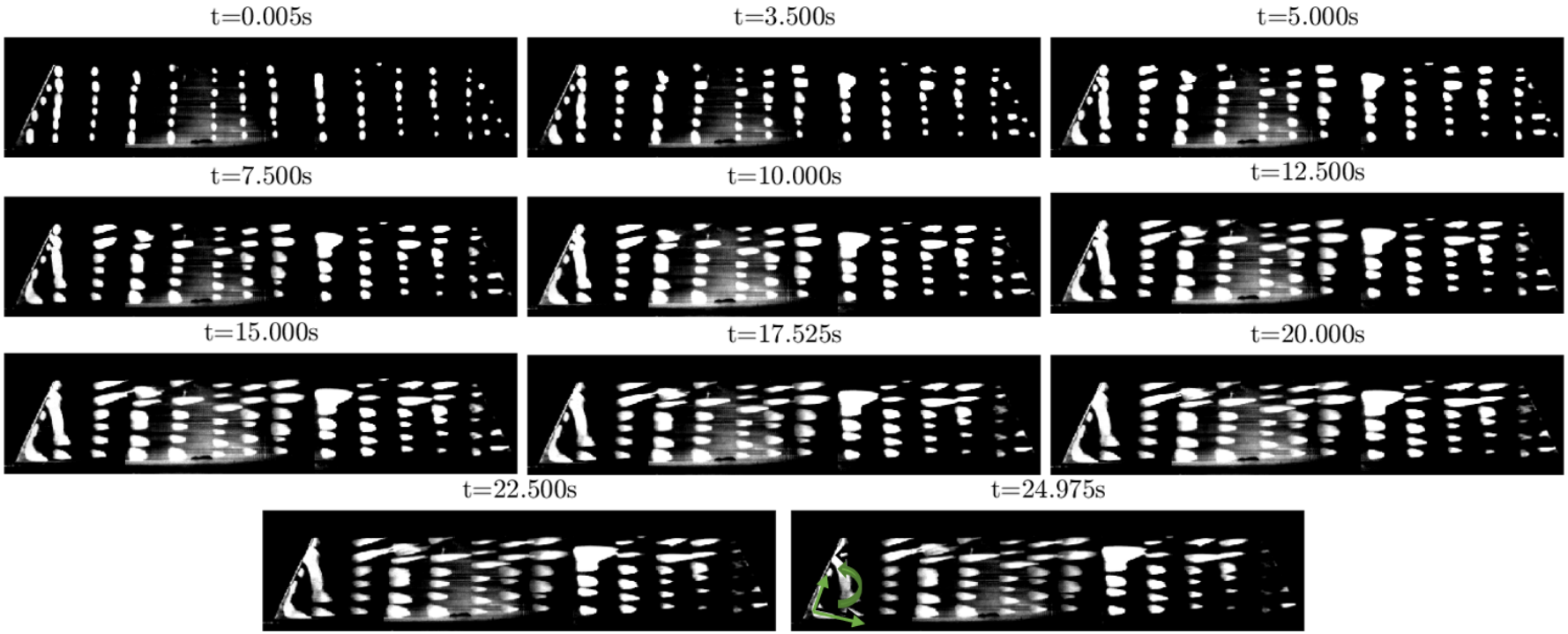

Figure 3-9: Flow evolution on the fin surface

The flow structures obtained from CFD simulations for flow over the SACOC fin are shown in Figure 3-10. Figure 3-10(a) and Figure 3-10 (b) are the zoomed in snippet to better visualize the leading edge flow structure developed showing the shear stress stream traces over the fin and the velocity stream traces on a sectional plane at 0.01 *mm* from the surface of the fin. It is observed from the two plots that the stream traces for velocity and shear stress are similar and within 10mm from the leading edge a recirculating region is seen from velocity stream traces and a straight shear stress distribution is observed in the shear stress distribution. Comparing this data to the experimental streak lines plotted in Figure 3-10, it is observed that a small recirculation region is observed at about 10mm from the leading edge, which is in good accordance with the CFD plots. The profile obtained from experimental data agrees closely to the shear stress distribution from Figure 3-10(a) which is appropriate as the oil droplets are applied on the surface on the fins and are assumed to depict the shear stress distribution, this comparison with the CFD results proves that the oil droplets in fact trace the shear stress distribution over a surface.

In order to further reinforce our assumption Figure 3-10(c) is used to compare the entire shear stress distribution over the fin results obtained from CFD to the experimental data and it is observed that the flow resembles the CFD results. We observe the same laminar like flow behavior 20mm from the bottom of the fin and a slight deflection towards the upper side of the fin at about 10mm from the top of the fin in both the experimental and CFD results.

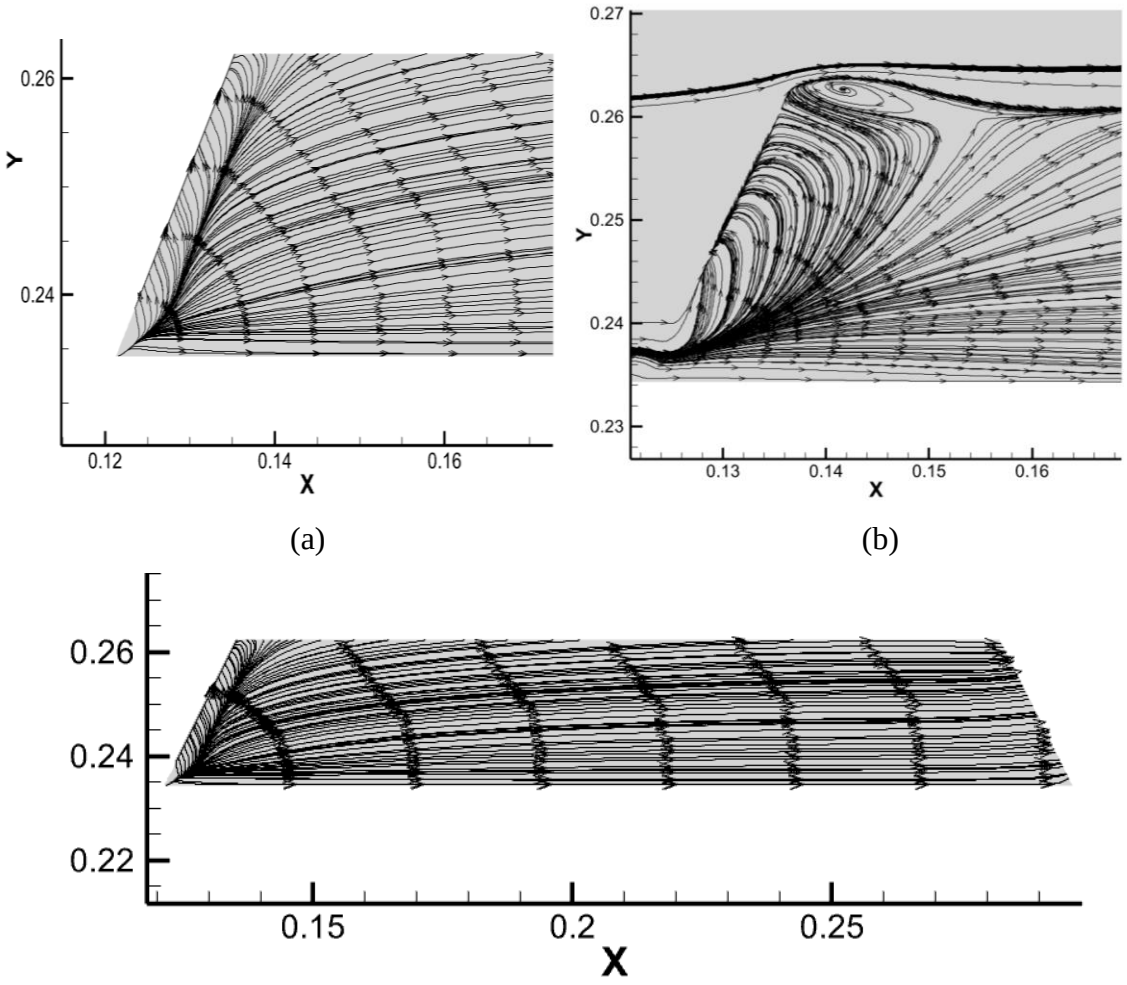

Figure 3-10: Flow structures obtained from CFD

Moving on to the results obtained from the top view at Mach 0.5. The time evolution history of the droplets is shown in Figure 3-11. The droplets at the bottom shear too quickly when compared to the droplets at the top in the frames below, reason being the different viscosities involved in the test. The droplets with lower viscosity respond much quicker to the incoming flow when compared to the high viscous droplets.

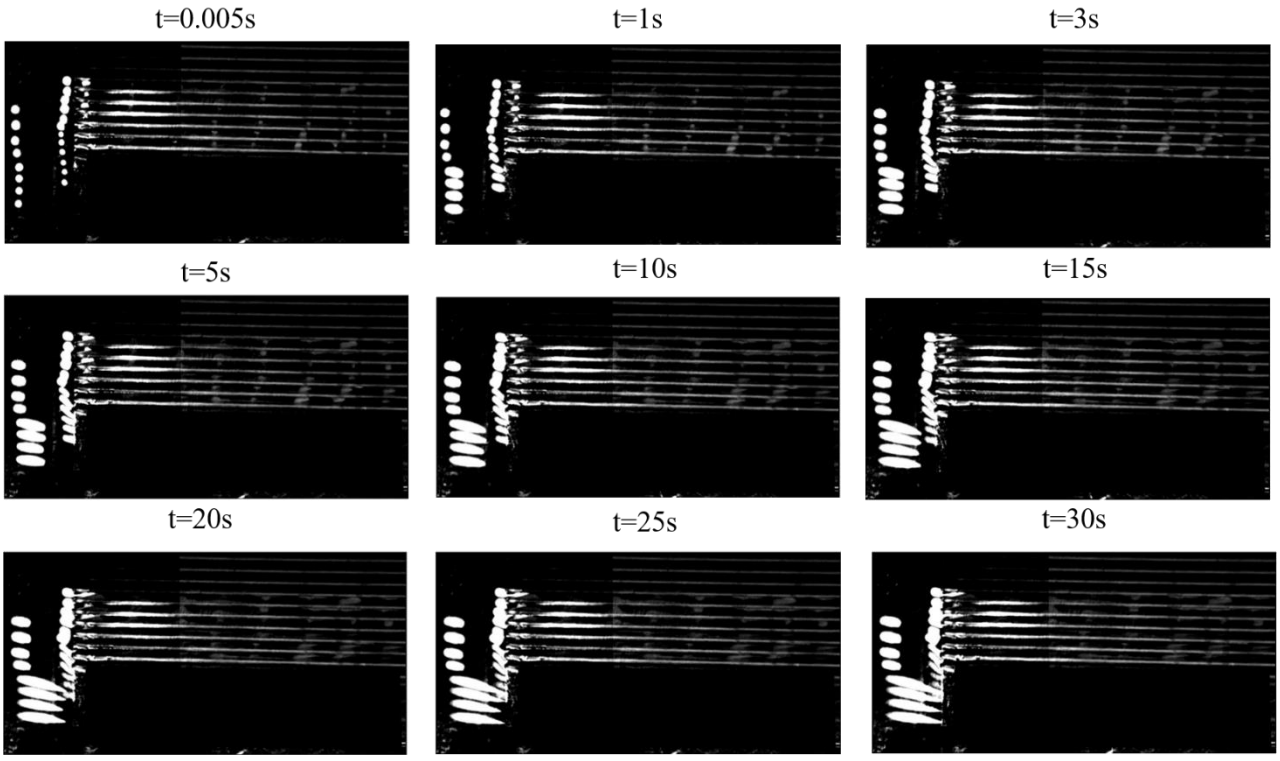

Figure 3-11: Secondary flow structure at the fins

The flow structure at the leading edge of the fins is summarized in Figure 3-12. There exists a small separation region right upstream of each fin. The high viscous oil droplets are marked in the final frame and from the time evolution it is evident that these droplets deform at a slower rate. Apart from the small separation at the leading edge, there is a slight deflection observed in the flow direction from the experimental data. As for the oil applied in between the fins, the oil droplets do deform with time, indicating the attached flow at all times in-between the fins. However, it is important to note that the oil dot deformation gives information at a point of application, there may be a separation and reattachment point in the region where the droplets may not have been placed. The experimental data captured validates with the CFD results, forming the similar flow structure, that is slight deflection of the flow also showing the separation region formation right upstream the fins.

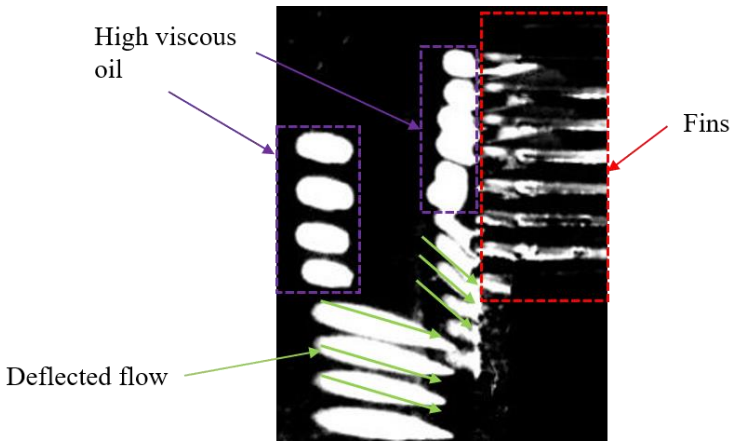

(a)

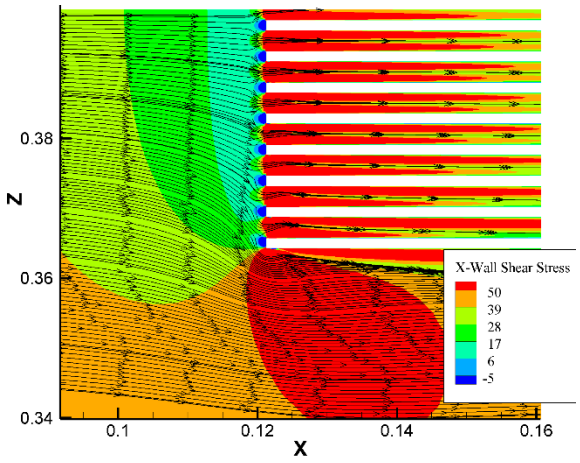

(b)

Figure 3-12: (a) Experimental flow structure (b) CFD at the leading edge of the fin at Mach 0.5

Figure 3-13 outlines the key flow aspects for at Mach 0.3 comparing the experimental and CFD results. A similar flow pattern as discussed for Mach 0.5 is observed. However, it is valuable to note the reduced deflection at the corner of the fins. This corner flow deflection is validated by the CFD results as can be observed from Figure 3-13(a). It is practical to have a flow deflection at the corner of the fins as there are secondary flow vortices generated due to the interaction of the flow with the fin which then pushes the flow away from the fins creating blockage. The Flow again remains attached to the surface at all times in between the fins as the oil droplets applied in between the fins are sheared. However, the applicability of these results depends on the obtained special resolution in between the fins.

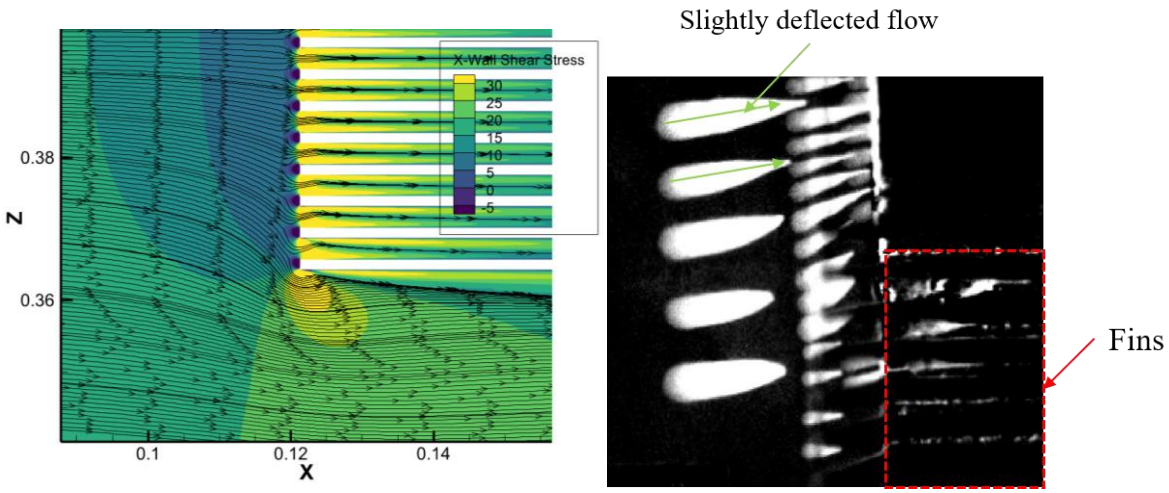

(a) (b)

Figure 3-13: (a) CFD results (b) Experimental results for bottom wall shear stress at Mach 0.3

A quantitative approach is followed by the qualitative analysis and the wall shear stress is calculated. It is now important to redo the order analysis considering the pressure gradients involved along the SACOC model. From the CFD results the local pressure gradient involved in the x-direction are extracted. As the some of the oil droplets are in the vicinity of the through flow and some are viewing the fins, a pressure gradient ranging from 3333 $pa\text{-}m^{-1}$ to 27500 $pa\text{-}m^{-1}$ are obtained for a Mach number of 0.3. Performing the order analysis with the same numbers from 2.1, we have the following new value for eq. 2.9. and the shear stress term we have an $O(10^{-8})$.

$$\frac{h^3}{3\mu}\frac{\partial P}{\partial x} = O(10^{-9}) - O(10^{-8}) \qquad 3\text{-}1$$

The pressure term is still an order of magnitude less than the shear stress term, however there are certain regions in the flow where the pressure term becomes as significant as the as the shear stress term meaning there are several regions in the test section where the tinning of the droplet may not be purely due to shear stress and there may be significant pressure forces acting on the droplet.

Performing the magnitude analysis for Mach 0.5, a similar trend is obtained. Pressure term is found to vary with a magnitude od O(10-6) to O(10-7), whereas the shear stress term has a magnitude of O(10-6). It is therefore observed that there are certain regions in the flow where the pressure forces are again significant. This region was identified to be the upstream of the fins and

it does make sense to expect high pressure variation upstream of the fins as the fins are blocking the main flow and the pressure is built up in the front of the fins.

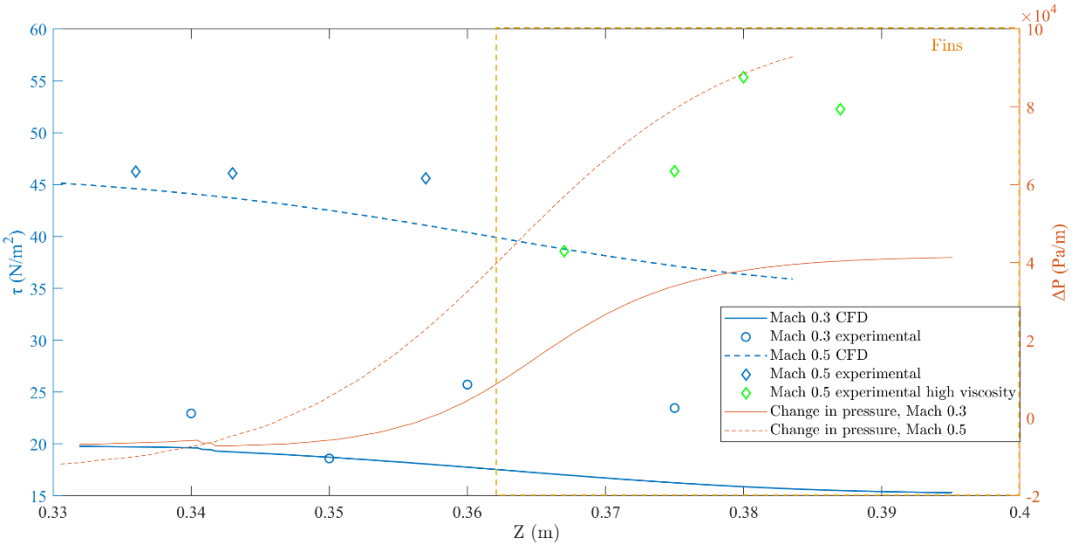

Figure 3-14: CFD and experimental results comparison

Experimental and CFD results obtained for SACOC are plotted in Figure 3-14. The results are compared in Z-direction. The CFD results were extracted from a K-omega SST simulations mimicking the experimental conditions. Change in pressure per unit length is plotted on the right y axis showing the variation of pressure built up in front of the fins. By looking at the plot it is clearly seen that there a significant variation of pressure along z – direction and hence the pressure forces acting on the droplet are significant at upstream the fins. The orange box on the plot resembles the region upstream of fins and is the region where the change is pressure per unit length is at peak.

Circle markers are the experimental results obtained for Mach 0.3 and the droplets far away from the fins are closer to the experimental data with an error of about 15% in the first droplet and about 0.3% for the second droplet and as observed from the plot the third and fourth droplets are closer to the fins where the pressure forces are significant which leads to about 44.5% rise in shear stress calculation. The experimental data however follows the decreasing trend as obtained from CFD simulations after an offset in shear stress.

Discussing the results for Mach 0.5, plotted with diamond markers on the plot, it is seen that the makers closely validate the CFD results with an error of 3% to 10%. The droplets deform

with a constant slope, failing to capture the decreasing trend in the shear stress as extracted from the CFD results. The markers marked with green are for the droplets of oil with higher viscosity and since these droplets are in the vicinity of high-pressure gradient region they are deviated from the shear stress CFD results. However, they do follow the decreasing shear stress trend with an initial offset in shear stress of about 24% which is further increased to about 50%.

Overall, from the figure it is observed that the experimental results are closely satisfying the CFD results where the pressure gradients are not high and clearly with an increase in Mach number an increase in shear stress is observed. Finally, for higher flow velocities, high viscous oil droplets provide better results. The deviation of experimental results from the CFD simulations maybe due to the reason that the shear stress along the plate just next to the fins is not purely one dimensional as this is one of the assumptions made for the shear stress computations for this technique and as seen clearly from flow visualization that the droplet does not exactly deform in x-direction and there is a slight deflection in the flow direction along x- direction.

3.3 Flow over turbine blade

It is quite interesting to be able to visualize the flow structures developed on the turbine blade and the turbine tip passage, on the other hand it is extremely difficult to set up a flow viz experiment to capture flow physics in the turbine blade and tip passage. In this section of the report an effort is made to capture the flow physics on the turbine blade at different AOA and the tip flows occurring at an AOA. It is important to note only one turbine blade was used in to capture the flow physics and it may not however accurately generate the flow as in an actual turbine passage. Additionally, the blade was fixed, and the relative flow measurements are not obtained, nevertheless it is possible to have the oil droplets deposited on the turbine tip rotated at a higher RPM and the frames captured with a high-speed camera can be used to extract the data wherein we see the turbine blade with the oil, disregarding all other frames. The limitation from this approach would be that the measurement thereby obtained are not true real time as the oil on the blade is not tracked continuously, but at a certain frequency. Nonetheless, data obtained will still be informative than obtaining a single frame at the end of the test.

3.3.1 Experimental set-up

Flow visualization testing was done on turbine blade and tip to characterize secondary flows. The setup consists of a simple *3in X 3in* optical test section to confine the airflow. The airflow was generated using a compressor at 130psi and a handheld blower was used to blow the air into the test section. The objective of this study is to track all the oil droplets on the surface of the turbine blade and characterize the flow field over the suction side of the turbine blade.

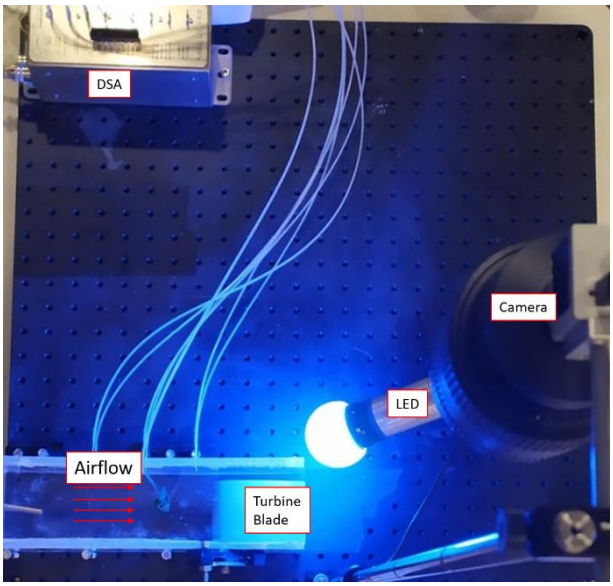

(a)

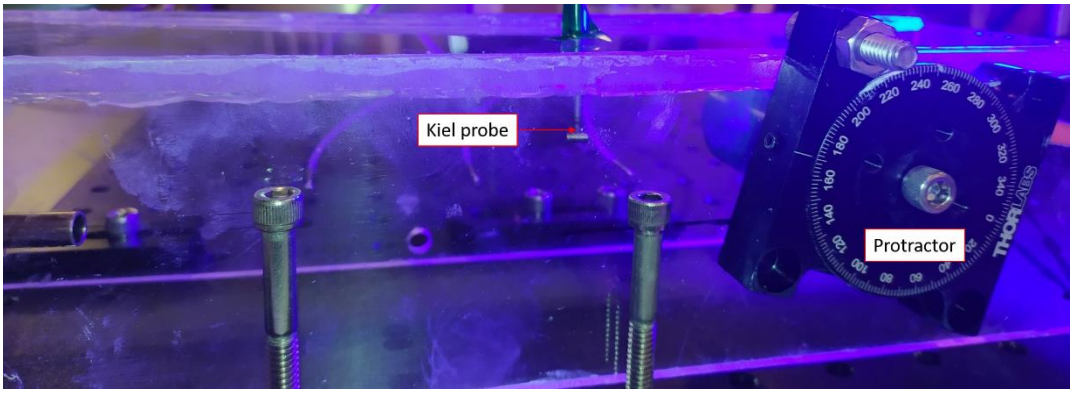

(b)

Figure 3-15: Experimental setup for turbine blade and tip flow

Figure 3-15 demonstrates the experimental setup. The turbine blade was mounted on a mechanical protractor that allowed to change the AOA of the turbine blade with a reference to

measure the angle. The test section is equipped with 6 static ports and one Kiel probe to measure the static and total pressure, respectively. A blue LED is used to illuminate the oil droplets and the Basler camera is used to record frames. The test section was manufactured using an acrylic sheet to ensure the optical access to the test section to be able to capture the oil data. The test condition is Mach 2. The span and chord of the turbine blade are 60.3 *mm* and 81.3 *mm* respectively, mounted with an angle of 18˚.

3.3.2 Results

Four tests were performed with the turbine blade, mounted at an angle of attack of 18˚, increasing the AOA in a step of 10˚, up to 48˚. Flow visualization was the primary objective of this experiment. Figure 3-16 reveals the flow evolution at 18˚. It is observed that the flow remains attached to the surface at all times through the center of the blade as all the droplets in this region deform. The rate of deformation is not constant and as seen the droplets at the leading edge deform quickly and the droplets applied at the trailing edge show very small deformation at a larger time, indicating that the shear stress is reduced moving along the chord of the blade. However, there is a separation region occurring at the edges of the turbine blade and can be observed as the droplets at the corners remain stagnant. The possible reason would be the developing vortex at the leading edge of the turbine blade which then extend onto the blade surface restricting the flow around the corners.

A video for this case as well as all other flow visualization at 4 different angles are included in the appendix section of the report, with the help of which these flow structures developed can be better understood.

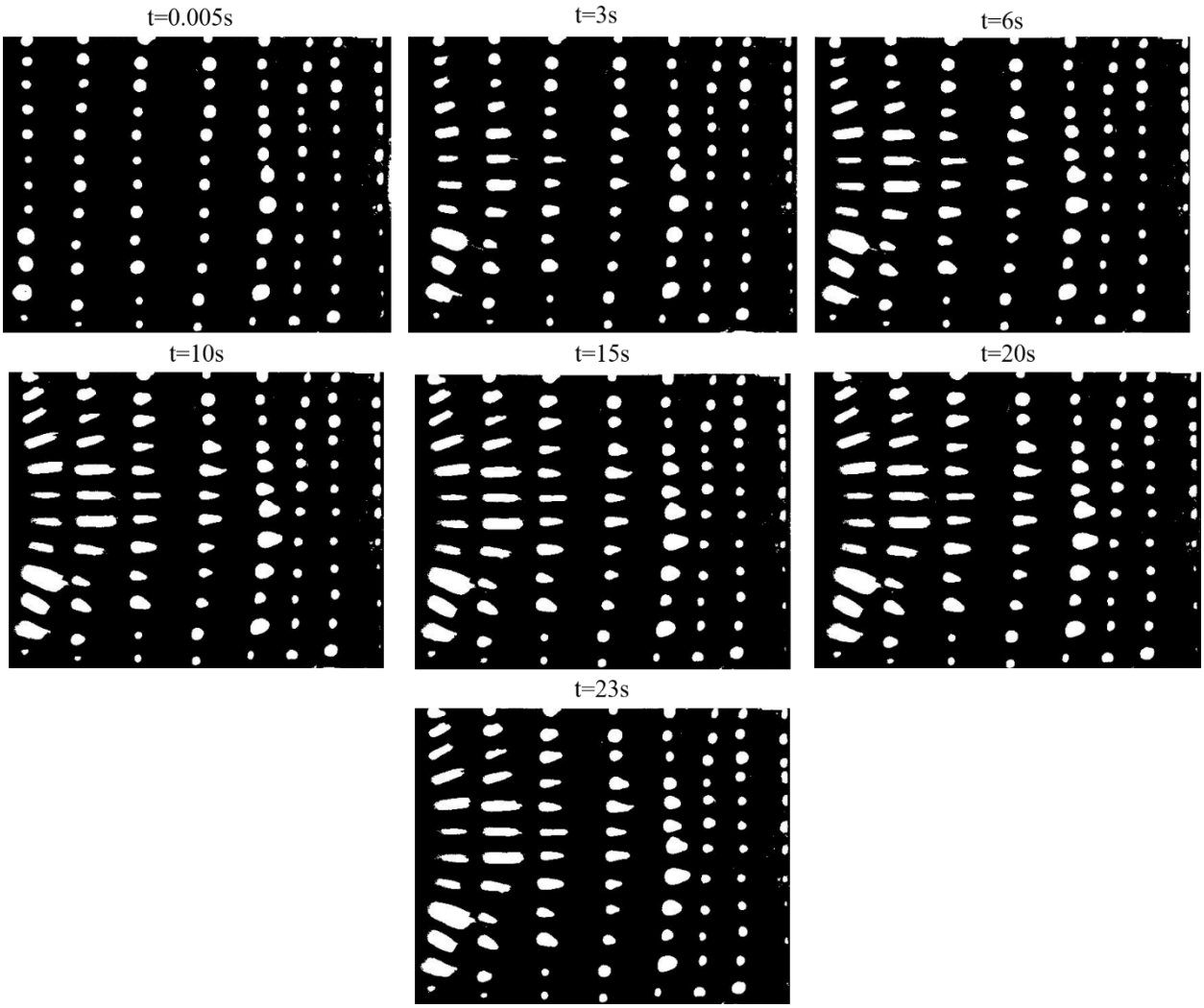

Figure 3-16: Flow evolution on turbine blade at 18˚

Another case for flow over the turbine blade at 48˚ is illustrated in Figure 3-17. In this case essentially the turbine surface is almost flat and in this case wall effects are observed. It is noted that the flow develops moving away from the center of the blade after a certain distance downstream the flow reflects from the walls of the test section and is seen to merge into the at the centerline of the blade. At initial times, the first-row droplets are seen to move away from the core flow and at a later time, these droplets tend to move towards the core flow, this illustrates the formation of the vortex structure at the leading-edge tip of the blade which then extends into the core flow on the blade surface. The droplets at the corners do not show any deformation indicating the separated region on the surface. The flow deflects from the walls of the test section thereby forming a separation along the blade surface closer to the corner of the test section.

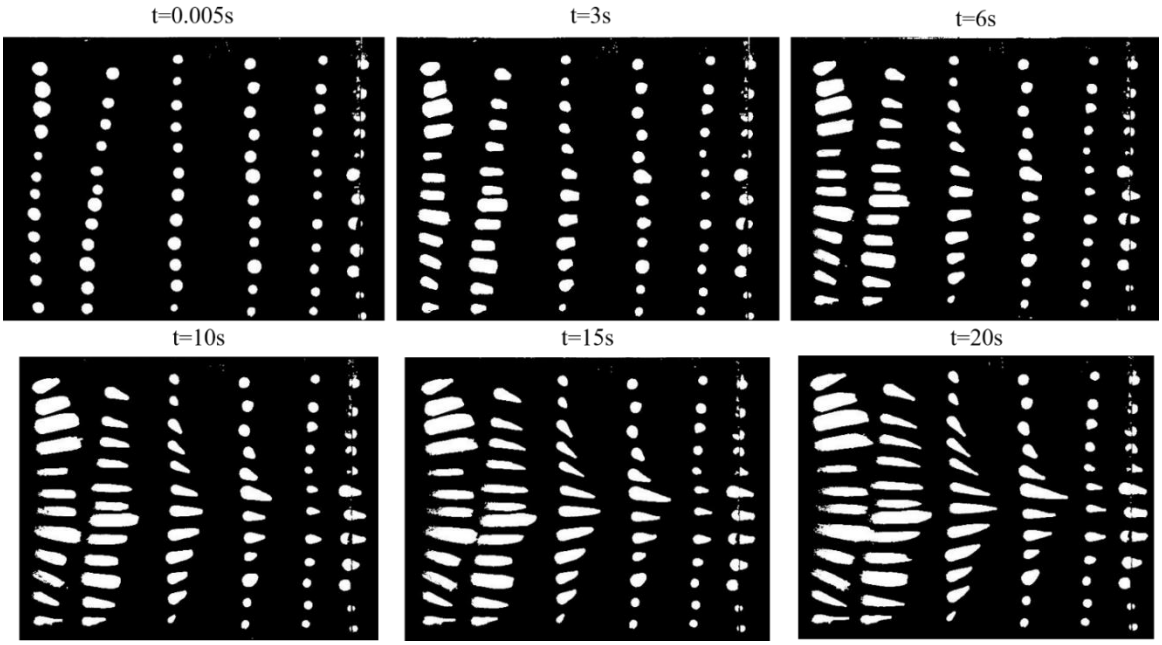

Figure 3-17: Floe evolution for turbine blade at 48˚

A quantitative streak line for the flow is demonstrated in Figure 3-18. The lines indicate the surface streak lines for the deformed droplet and the circles indicate the separation region on the blade as the oil droplets at those regions do not deform. The reason for this being the flow structure developed from the leading edge of the turbine blade and the reflected flow from the wall that tend to form at the center of the blade.

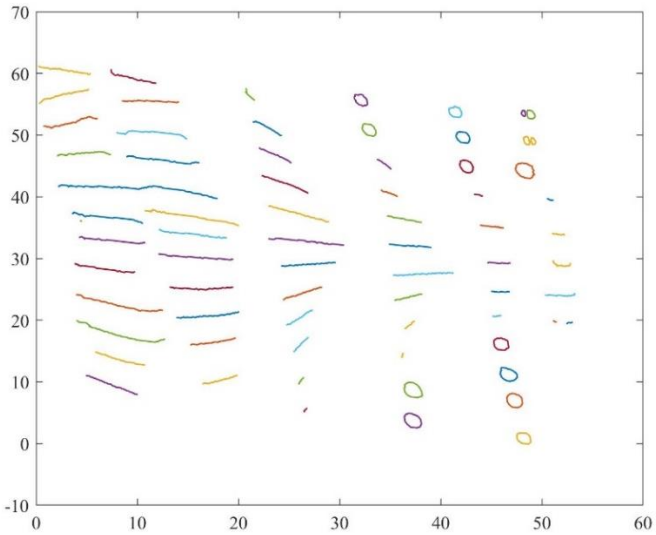

Figure 3-18: Surface streak lines for flow over turbine blade

4. CONCLUSIONS

Two different methodologies were developed, compared, and studied to calculate the shear stress using the oil drop technique. One of which includes processing frames captures during the test whereas the other method is to track a droplet from a processed undistorted video. Processing frames offered more flexibility to play with each frame and obtain a binary image before detecting the oil droplet boundaries. The video processing however did not allow much flexibility and a grayscale video was used to track a droplet. The droplet boundaries were found to be accurately deciphered using the frame processing approach as for each frame new set of points are defined. In case of video processing, the tracked points depend on the data from the previous frame and any vibrations captured by the camera resulted in errors in accurately tracing the droplet boundaries. The developed frame processing MATLAB routine works best for all cases with the assumptions and calibration methodology developed. An uncertainty quantification is performed, and the results obtained using this technique seem to lie within an uncertainty of <4%. Maximum uncertainty is found to be induced by the MATLAB processing routine, followed by the oil volume dispensed and droplet deformed length calculations. Hence it is very important to precisely calculate the deformed oil droplet length and use appropriate methodology to detect the droplet boundaries. It is also equally important to precisely apply the right amount of volume on the model surface.

With the undistorted frames used for tracking the droplets, the skeleton image for the deformed oil droplet is computed and a mapping routine is employed to convert the detected deformed droplet boundaries to real world coordinates. Finally, these coordinates are plotted as surface streak lines, capturing the flow structures at the wall. Same data obtained for shear stress calculations is used to plot the streak lines, therefore, reducing the number of tests to be performed, multiple equipment's, uncertainty due to repeatability and certainly the data processing and storage requirements which would otherwise be necessary for two different approaches.

The obtained results are first compared with an empirical correlation for the case of a flat plate and the results are satisfying with the calculated empirical correlations. It is found that the experimental results lie within 95% confidence interval for the theoretical calculations. The second case studied was flow over SACOC fins and the experimental data is compared with the CFD results. A total of 3 different tests are performed in this experimental campaign. To capture the

flow structure on the side of the fin at Mach 0.3, to capture the flow structure and calculate the shear stress upstream and in between fins at Mach 0.3 and Mach 0.5. The flow visualization results compared with the CFD results for the flow over the fin exactly match the flow structures captured by the CFD data. The secondary flows occurring at the leading edge and the flow pattern on the entire surface of the fin are in great agreement CFD results. The flow visualization performed upstream and in between the fins show a slight deflection in the flow pattern beside the fins which is not captured in the CFD results. Lastly, the shear stress was calculated upstream the fins and is compared with the CFD data. The experimental shear stress is found to be within 15% percent of the CFD data for Mach 0.3 flow and the data lies in the range of 3 to 10% for Mach 0.5 flow.

An additional flow viz experiment on the turbine blade is carried out to demonstrate separation occurring on the surface of a turbine blade at different angle of attacks.

APPENDIX A

Flow over the surface of the fin

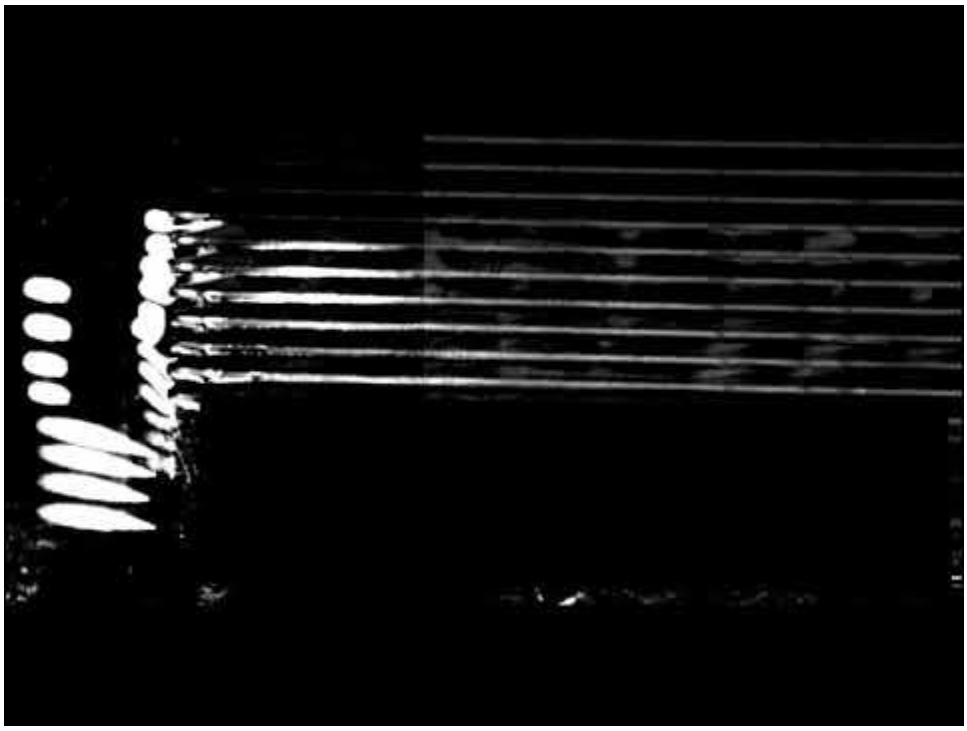

Flow on the bottom plate of the fins

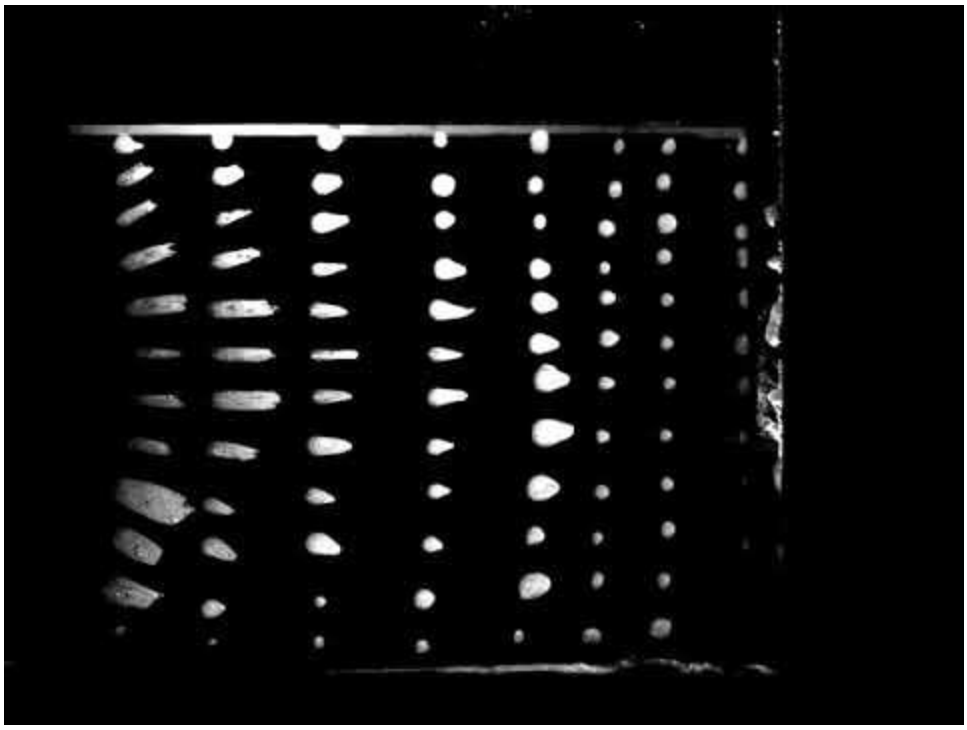

Flow over turbine blade at 18 ˚

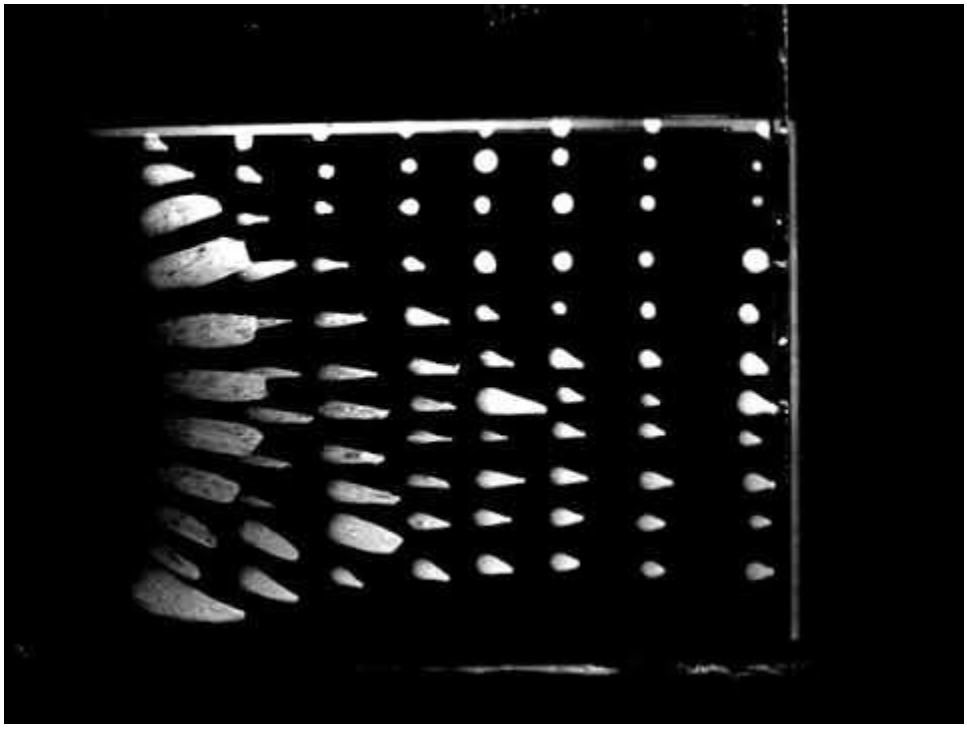

Flow over turbine blade at 28 ˚

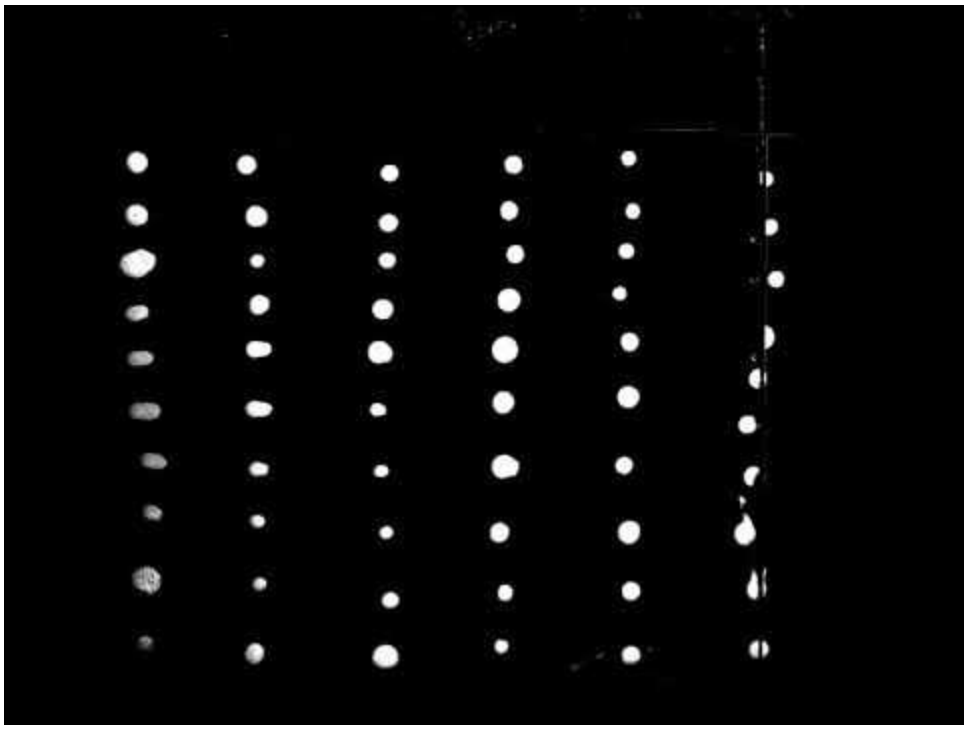

Flow over turbine blade at 38 ˚

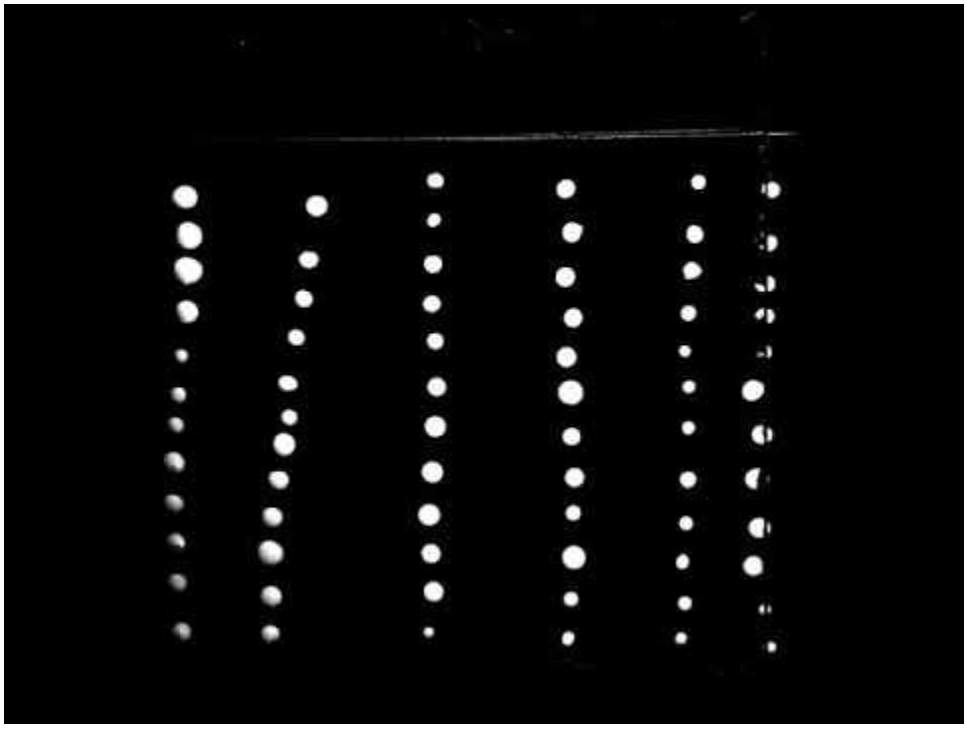

Flow over turbine blade at 48 ˚

APPENDIX B. MATLAB CODE

Code used to undistort frames:

```
%%%%%%%%%%%%%%%%%%%%%%%%%%%%%%%%$%%%%%%%%%%%%%%%%%%%%%%
%%%%%%%%%%%%%%%%%% Syed Shoiab %%%%%%%%%%%%%%%%%%%%%%%%
%%% Camera calibration and frame undistorion script %%%
%%%%%%%%%%%%%%%%%%%%%%%%%%%%%%%%%%%%%%%%%%%%%%%%%%%%%%%

clc
clear

images = imageDatastore('file_directory');

[imagePoints,boardSize] =
detectCheckerboardPoints(images.Files);

squareSize = 3;
worldPoints = generateCheckerboardPoints(boardSize,squareSize);

IC = readimage(images,2);
imagepoints=detectCheckerboardPoints(IC);
imageSize = [size(IC,1),size(IC,2)];
% cameraParams =
estimateCameraParameters(imagePoints,worldPoints,'ImageSize',ima
geSize);
[cameraParams,imagesUsed,estimationErrors] =
estimateCameraParameters(imagePoints,worldPoints);

[IMC, newOrigin] =
undistortImage(IC,cameraParams,'OutputView','full');
% [IMC, newOrigin] =
undistortFisheyeImage(IC,cameraParams.Intrinsics);
% %used to undistort Fisheye errors
figure; showReprojectionErrors(cameraParams);
title('Reprojection Errors');

%{
To map points in the image coordinates to points in the world
coordinates
we need to compute the rotation and the translation of the
camera relative
to the calibration pattern. Note that the extrinsics function
assumes that
there is no lens distortion. In this case imagePoints have been
detected in
```

```
an image that has already been undistorted using undistortImage.
%}

[imagePoints,boardSize] = detectCheckerboardPoints(IMC);
imagePoints = imagePoints + newOrigin; % adds newOrigin to every
row of imagePoints

% Compute rotation and translation of the camera.
[R, t] = extrinsics(imagePoints, worldPoints, cameraParams);
WorldPoints = pointsToWorld(cameraParams,R,t,imagePoints);
worldpoints = pointsToWorld(cameraParams,R,t,imagepoints);

figure
plot(worldPoints(:,1),worldPoints(:,2),'gx');
hold on
plot(WorldPoints(:,1),WorldPoints(:,2),'bo');
hold on
plot(worldpoints(:,1),worldpoints(:,2),'ro');
legend('True points','Calibrated points','Distorted points');
hold off

%{
%routine to calaulate errors
err_x=(worldPoints(:,1)-WorldPoints(:,1));
maxerr_x=max(abs(err_x));
err_y=(worldPoints(:,2)-WorldPoints(:,2));
maxerr_y=max(abs(err_y));
%}
%%

path = 'path_to_distorted_frames';
savepath = 'Path_where_undistorted_frames_to_be_saved';

%%
frame = 1101;frameno=1;
% AA=[901:1:10000]; %use this if frame sampling is required
sc = 8; %%% TO MAKE IT MORE BRIGHT INCREASE THE SC ( was 8
before)
%%
while frame<9001
%     if ismember(frame,AA);
    imref = imread(strcat(path,'background_image_saved_name'));
    imgor =
imread(strcat(path,'frames_saved_name',num2str(frame),'.tiff'));
    img = imgor-imref;
    img=double(img);
    %sc = 8*32;
```

```
%     img=img(y1:y2,x1:x2); %use this line if cropping the
original frame
%     J2 = undistortImage(img,cameraParams,'OutputView','full');
    im1 = mat2gray(img); %converts the matrix A to an intensity
image I that contains values in the range 0 (black) to 1
(white).
 %{
    %Use this block to divide the image for threshold and stitch
    im1a = im1(:,1:450);
    im1b = im1(:,451:620);
    im1c = im1(:,621:800);
    im1a = mat2gray(im1a, [0.0 0.25]);
    im1b = mat2gray(im1b, [0.05 0.3]);
    im1c = mat2gray(im1c, [0.05 0.2]);
    im2 = [im1a, im1b, im1c];
    %end of stitching block
 %}
%{
    %Use this block to divide the image for threshold and stitch
y
    im1a = im1(1:275,:);
    im1b = im1(276:632,:);
%     im1c = im1(:,610:800);
    im1a = mat2gray(im1a, [0.5 1]);
    im1b = mat2gray(im1b, [0.1 0.35]);
%     im1c = mat2gray(im1c, [0.6 0.95]);
    im2 = [im1a; im1b];%, im1c];
    %end of stitching block
    %use the next line to threshold without stitching
%}
    %{ Use this block to obtain a ROI mask if required (mostly
done in later routine)
%     objectRegion=roipoly(im1);
%     maskedROIImage = bsxfun(@times, im2, cast(~objectRegion,
'like', zeros));
%     whos maskedROIImage;
%}
     %play with threshold to get a good visual
    im2 = mat2gray(im1, [0.05 0.3]); %play with threshold to get
a good visual
%     figure
%     imshow(im1)

%     [imc, newOrigin] = undistortImage(I,cameraParams);

    J2 = undistortImage(im2,cameraParams,'OutputView','full');
```

```
%
imwrite(J2,strcat(savepath,num2str(frameno),'.tiff')); %saves
tiff
%     frame
    save(strcat(savepath,num2str(frameno)),'J2');  %saves .mat
image file
    frameno=frameno+1;
%     end
    frame=frame+1;

end

% change the threshold for end frames to get better viz
%{
while frame<28265
    img =
imread(strcat(path,'fimename',num2str(frame),'.tiff'));

    img=double(img);
    %sc = 8*32;
%     img=img(y1:y2,x1:x2);
%     J2 = undistortImage(img,cameraParams,'OutputView','full');
    im1 = mat2gray(img); %converts the matrix A to an intensity
image I that contains values in the range 0 (black) to 1
(white).

%     im1 = mat2gray(im1, [0 0.65]); %play with threshold to get
a good visual
%     im1 = mat2gray(im1, [0.9 1]); %play with threshold to get
a good visual
    im1 = mat2gray(im1, [0.45 0.75]);
%     figure
%     imshow(im1)

%     [imc, newOrigin] = undistortImage(I,cameraParams);

%     [imc, newOrigin] =
undistortImage(im1,cameraParams,'OutputView','full');

    J2 = undistortImage(im1,cameraParams,'OutputView','valid');

%     imwrite(J2,strcat(savepath,num2str(frameno),'.tiff'));
    save(strcat(savepath,num2str(frameno)),'J2');
    frameno=frameno+1;
%     end
    frame=frame+1;
end
```

```
%}
save(strcat(savepath,'data.mat'),'cameraParams','R','t','frameno
','newOrigin','estimationErrors');
```

Code used to track droplet:

```
%%%%%%%%%%%%%%%%%%%%%%%%%%%%%%%%%%%%%%%%%%%%%%%%%%%%%%%%%%%%%%%%%%%%%%%
%%%%%%%%%%%%%%%%%%%%%%%%%%%%%%%%%%%%%%%%%%%%%%%%%%%%%%%%%%%%%%%%%%%%%%%
%%%%%%%%%%%%%%%%%%%%%%%%%%% Syed Shoiab %%%%%%%%%%%%%%%%%%%%%%%%%%%%%%%%
%%% Frame and VIdeo processing routine to obtain thinning rate %
%%%%%%%%%%%%%%%%%%%%%%%%%%%%%%%%%%%%%%%%%%%%%%%%%%%%%%%%%%%%%%%%%%%%%%%

clc;clear
%%
nob = 1; %number of tracking droplets
%{
Kin_vis = 1000; %viscosity of oil cst
rho = 970; % density of oil used (silicone oil- 970kg/m3 @25C)
D_vis = Kin_vis*10^(-6)*rho; %(m2/s)
%}
% V = 1; %volume in microlitre same as mm3
path = 'undistorted frames path';
savepath='savepath for thinning rate';
videosavepath='savepeth for thinning rate from video
processing';
load('load data file from camera calibration')
videoReader = VideoReader('.avi file path');
filename = 'filename.csv';
frames = floor(videoReader.Duration*videoReader.FrameRate);
dt=1/videoReader.FrameRate;%frames/(videoReader.Duration*videoRe
ader.FrameRate);
v = VideoWriter('tracked_video.avi');%,'Grayscale AVI');
videoPlayer = vision.VideoPlayer;


%% TO track frames

%Routine to track thinning rate using frames
for ii=1:nob
    LLL=1;
    figure;
    load(strcat(path,num2str(frameno-1),'.mat'));
    % load(strcat(path,'4901.mat'));
    figure;imshow(J2);
    title('Seclect the region of interest');
    objectRegion=roipoly(J2);
    hold on;
    % objectRegion=drawrectangle(J2);
    % objectRegion=round(getPosition(imrect));
    V = input('Enter drop Volume in mm^3=');
    %for kk=1:10:200
    gtv=[1:100:9000];
```

```
    gtv22=1;

    while gtv22<length(gtv)
        clear idx boundarypoints boundaries B I worldpoints
        kk=gtv(gtv22);
    %     kkk=gtv(gtv22+1);
    %     load(strcat(path,num2str(kk),'fringe.mat'));
        load(strcat(path,num2str(kk),'.mat'));
    %     load(strcat(path,num2str(1),'.mat'));
        time(LLL,1)=(kk-1)*dt;
        %str = strcat(path,num2str(jj),'.mat'); load(str);
        % Masking image
        maskedROIImage = bsxfun(@times, J2, cast(objectRegion,
'like', zeros));
        whos maskedROIImage;
    %     figure(1)
        img=double(maskedROIImage);
        %sc = 8*32;

        BWs=edge(img,'Prewitt');    %use different methods to
get proper edges, like Prewitt, Canny, Sobel, Roberts
    %     imfreehand=getPosition(J2);
    %     figure;
    %     imshow(BWs);

        se90 = strel('line',3,90); %creates a structural
element, here line of length 3 and 90 degree
        se0 = strel('line',3,0);
        BWsdil = imdilate(BWs,[se90 se0]);
    %     figure
    %     imshow(BWsdil)
    %     title('Dilated Gradient Mask')

        BWdfill = imfill(BWsdil,'holes');
    %     figure
    %     imshow(BWdfill)
    %     title('Binary Image with Filled Holes')

        BWnobord = imclearborder(BWdfill,8);
    %     figure
    %     imshow(BWnobord)
    %     title('Cleared Border Image')
    %{
        seD = strel('diamond',1);
        BWfinal = imerode(BWnobord,seD);
        BWfinal = imerode(BWfinal,seD);
```

```
%     BWfinal = imerode(BWdfill,seD);
    figure;
    imshow(BWfinal)
    title('Segmented Image');

    BWoutline = bwperim(BWfinal);
    Segout = img;
    Segout(BWoutline) = 255;
    figure
    imshow(Segout)
    title('Outlined Original Image')

    boundary = bwtraceboundary(BWfinal,[100, 129],'N');
    figure;
    imshow(img)
    hold on;
    plot(boundary(:,2),boundary(:,1),'g','LineWidth',2);
    boundary = boundary+newOrigin;
%}

%     boundaries = bwboundaries(maskedROIImage,'noholes');
    boundaries = bwboundaries(BWnobord,'noholes');
    bds=size(boundaries);
    bds=bds(1);

    for jj=1:bds
        arr=(cell2mat(boundaries(jj)));
        idx(jj,1:2)=size(arr);
    end
    idx=idx(:,1);
    [B I] = sort(idx, 'Descend');

%{
    %block to plot boundaries
    hold on;
    for ii=1:1
    pp=cell2mat(boundaries(ii,1));
    plot(pp(:,2),pp(:,1));
    hold on;
    end
%}

    boundarypoints=boundaries(I(1));
    boundarypoints=cell2mat(boundarypoints);
    plot(boundarypoints(:,2),boundarypoints(:,1));
    boundarypoints = boundarypoints+newOrigin;
```

```
%         worldpoints(1:B(ii),jj:jj+1) =
pointsToWorld(cameraParams,R,t,boundarypoints);
         worldpoints(LLL,ii) =
{pointsToWorld(cameraParams,R,t,boundarypoints)};
%         jj=jj+2;
        worldpts = cell2mat(worldpoints(LLL,ii));
        polyin = polyshape([worldpts(:,1)],[worldpts(:,2)]);
        A(LLL,ii) = area(polyin);
        L(LLL,ii) = abs(max(worldpts(:,2)))-
abs(min(worldpts(:,2)));
        W(LLL,ii) = abs(max(worldpts(:,1)))-
abs(min(worldpts(:,1))); %Use Pythagoras theorem to get tangent
        %Next 3 lines for uncertainty quantification
%         W(LLL,ii) = abs(max(worldpts(:,1)))-
abs(min(worldpts(:,1)));
%         L(LLL,ii) = L(LLL,ii)+0.23;
%         A(LLL,ii) = A(LLL,ii)+(0.23*W(LLL,ii));
        %{
        %if assuming hemispherical shape
        if gtv22<10    %assuming the droplet is hemispherical
until 16 seconds
            h(LLL,ii) = A(LLL,ii)/pi;
            h(LLL,ii) = sqrt(h(LLL,ii));
            V=A(LLL,ii)*(2/3)*h(LLL,ii);
%             V1=(2/3)*pi*h(LLL,ii)^3;
        else
            h(LLL,ii) = 2*V/(0.9*A(LLL,ii));
        end
        %}
        %{
        %Use this block if the volume of the droplet is known
        h(LLL,ii) = V/A(LLL,ii);
        if gtv22<20
           h(LLL,ii)=(3/2)*h(LLL,ii);
        else
            h(LLL,ii)=2*h(LLL,ii);
        end
        %}

        %If using spherical cap assumption with known volume

        if gtv22<1     %assuming the droplet doesn't move for 16
seconds
            syms a
            eqn = V==(1/6)*pi*a*(3*(L(LLL,ii)/2)^2 + a^2);
            hh(LLL,ii) = solve(eqn,a,'Real',true);
            h(LLL,ii) = sym2poly(hh(LLL,ii));
```

```
        else
            h(LLL,ii) = 2*V/(A(LLL,ii)*0.95);
        end
        %}
        %{
        %for cylindrical shape assumption
        if gtv22<10
            h(LLL,ii)=V/A(LLL,ii);
        else
            h(LLL,ii)=2*V/(A(LLL,ii)*0.9);
        end
        %}
%         L = max(worldpts(:,2)) - min(worldpts(:,2));

        ratio(LLL,ii) = (0.95*L(LLL,ii))/h(LLL,ii);
    %     end
    %     if ii==1
    %
save(strcat(savepath,'datapoints',num2str(kk),'.mat'),'worldpoin
ts');
    %     else
    %
save(strcat(savepath,'datapoints',num2str(kk),'.mat'),'worldpoin
ts','-append');
    %     end
        LLL=LLL+1;
        gtv22=gtv22+1;

    end
end
%}

%% Save Frame data

%
save(strcat(savepath,'datapoints',num2str(kk),'.mat'),'worldpoin
ts');
save(strcat(savepath,'sheardata.mat'),'time','A','h','L','ratio'
);
cHeader = {'time1' 'Area1' 'area2' 'area3' 'area4' 'area5'
'height1' 'h2'...
    'h3' 'h4' 'h5' 'Length1' ' L2' 'L3' 'L4' 'L5' 'L/h1'
'l/h2'...
    'l/h3' 'l/h4' 'l/h5'}; %dummy header
commaHeader = [cHeader;repmat({','},1,numel(cHeader))]; %insert
commaas
commaHeader = commaHeader(:)';
```

```
textHeader = strjoin(cHeader, ','); %cHeader in text with commas
%write header to file
fid = fopen(strcat(savepath,filename),'w');
fprintf(fid,'%s\n',textHeader);
fclose(fid);
%write data to end of file
xlswrite(strcat(savepath,filename),time,1,'A2');
xlswrite(strcat(savepath,filename),A,1,'B2');
xlswrite(strcat(savepath,filename),h,1,'G2');
xlswrite(strcat(savepath,filename),L,1,'L2');
xlswrite(strcat(savepath,filename),ratio,1,'Q2');
clear time A h L ratio worldpoints worldpts
%% TO track video

%block to select and process ROI
objectFrame = read(videoReader, frames);
% J2e=objectFrame(:,:,1);
% BWs=edge(J2e);
% se90 = strel('line',3,90); %creates a structural element, here
line of length 3 and 90 degree
% se0 = strel('line',3,0);
% BWsdil = imdilate(BWs,[se90 se0]);
% BWdfill = imfill(BWsdil,'holes');
% BWnobord = imclearborder(BWdfill,8);
figure
binimg=imbinarize(objectFrame);%,'adaptive','ForegroundPolarity'
,'bright','Sensitivity',0.35);
objectRegion=roipoly(binimg); %select the region that you do not
intend/or intend to keep
%in the image(noise or ROI)

% objectRegion = (~objectRegion); %Use this line if selecting
noise for masking else comment this line
maskedROIImage = bsxfun(@times, binimg, cast(objectRegion,
'like', zeros));
whos maskedROIImage;

boundaries = bwboundaries(maskedROIImage,'noholes');
%masking image
% figure;imshow(BWnobord)
% maskedROIImage = bsxfun(@times, BWnobord, cast(objectRegion,
'like', BWnobord));
% whos maskedROIImage;
% boundaries = bwboundaries(maskedROIImage,'noholes');
bds=size(boundaries);
bds=bds(1);
bds=size(boundaries);
```

```
bds=bds(1);
% LLL=1;

for ii=1:bds
    arr=(cell2mat(boundaries(ii)));
    idx(ii,1:2)=size(arr);
end
idx=idx(:,1);
[B I] = sort(idx, 'Descend');

jj=1;
for kk=1:nob
    points=boundaries(I(kk));
    points=cell2mat(points);
%     boundarypoints = boundarypoints+newOrigin;
%         worldpoints(1:B(ii),jj:jj+1) =
pointsToWorld(cameraParams,R,t,boundarypoints);
%     worldpoints(ii) =
{[pointsToWorld(cameraParams,R,t,boundarypoints)];};
%         jj=jj+2;

    n=size(points);
    n=n(1);

    points = [points(:,2) points(:,1)];
    pointImage =
insertMarker(objectFrame,points,'+','Color','red');
    figure;
    imshow(pointImage);
    title('Detected interest points');
    prompt ='Enter 1 to track this blob or enter to skip';
    tf = input(prompt);
    if tf == 1
%         track=1;
%         while track<3
%
        LLL=input('Enter the blob tag');
        V = input('Enter drop Volume in mm^3=');
        % Create a tracker object.
        open(v);
        tracker =
vision.PointTracker('MaxBidirectionalError',1);
        initialize(tracker,points,objectFrame);
        % while ~isDone(videoFileReader)
        for ii = frames:-1:1
        %     frame = videoFileReader();
```

```
%             time(frames-ii+1,1) =
videoReader.CurrentTime;%(ii-1)*dt;
            time(ii,LLL) = videoReader.CurrentTime;%(ii-1)*dt
            frame = read(videoReader, ii);
            [trackedpoints,validity] = tracker(frame);
            ValidPoints = trackedpoints(validity,:);
            sz = size(ValidPoints);
            sz = sz(1,1);
            mm=1;
            for jj=1:sz
              validpoints(1,mm) = ValidPoints(jj,1);
              validpoints(1,mm+1) = ValidPoints(jj,2);
              mm=mm+2;
            end
            Validpoints(ii,LLL) = {ValidPoints};
            %
setPoints(vision.PointTracker,points)%,validity)
            out =
insertMarker(frame,trackedpoints(validity, :),'+','color','green
');
            outline =
insertShape(frame,'line',validpoints,'LineWidth',3);
            %       videoPlayer(outline);
            videoPlayer(out);

            boundarypoints = Validpoints(ii,LLL);
            boundarypoints=cell2mat(boundarypoints);
%             plot(boundarypoints(:,1),boundarypoints(:,2));
            boundarypoints = boundarypoints+newOrigin;
    %         worldpoints(1:B(ii),jj:jj+1) =
pointsToWorld(cameraParams,R,t,boundarypoints);
             worldpoints =
{pointsToWorld(cameraParams,R,t,boundarypoints)};
    %         jj=jj+2;
            worldpts = cell2mat(worldpoints);
            polyin = polyshape([worldpts(:,1)],[worldpts(:,2)]);
            A(ii,LLL) = area(polyin);
            L(ii,LLL) = abs(max(worldpts(:,1)))-
abs(min(worldpts(:,1)));

 %{
            %if assuming hemispherical shape
%             V=(2/3)*pi*(L(ii,LLL)/2)^3;
            if ii==frames
                frame1 = read(videoReader, 1);
                frame1=imbinarize(frame1);
```

```
                maskedROIImage = bsxfun(@times, frame1,
cast(objectRegion, 'like', zeros));
                whos maskedROIImage;
                img=double(maskedROIImage);
                BWs=edge(img,'Prewitt');    %use different
methods to get proper edges, like Prewitt, Canny, Sobel, Roberts
                se90 = strel('line',3,90); %creates a structural
element, here line of length 3 and 90 degree
                se0 = strel('line',3,0);
                BWsdil = imdilate(BWs,[se90 se0]);
                BWdfill = imfill(BWsdil,'holes');
                BWnobord = imclearborder(BWdfill,8);
                boundaries = bwboundaries(BWnobord,'noholes');
                bds=size(boundaries);
                bds=bds(1);
                for jj=1:bds
                    arr=(cell2mat(boundaries(jj)));
                    idx(jj,1:2)=size(arr);
                end
                idx=idx(:,1);
                [B I] = sort(idx, 'Descend');
                boundarypoints=boundaries(I(1));
                boundarypoints=cell2mat(boundarypoints);
                boundarypoints=boundarypoints+newOrigin;
                worldpoints =
{pointsToWorld(cameraParams,R,t,boundarypoints)};
                worldpoints = cell2mat(worldpoints);
                polyin =
polyshape([worldpoints(:,1)],[worldpoints(:,2)]);
                A1 = area(polyin);
                L1 = abs(max(worldpoints(:,1)))-
abs(min(worldpoints(:,1)));
                V=A1*(2/3)*(L1/2);
            end
            if time(ii,LLL)<0.06    %assuming the droplet is
hemispherical until 16 seconds
                h(ii,LLL) = A(ii,LLL)/pi;
                h(ii,LLL) = sqrt(h(ii,LLL));
                V1=A(ii,LLL)*(2/3)*h(ii,LLL);
    %             V1=(2/3)*pi*h(ii,LLL)^3;
            else
                h(ii,LLL) = 2*V/(0.9*A(ii,LLL));
            end
            %}
            %{
            %Use this block if the volume of the droplet is
known
```

```
            h(LLL,ii) = V/A(LLL,ii);
            if gtv22<20
               h(LLL,ii)=(3/2)*h(LLL,ii);
            else
                h(LLL,ii)=2*h(LLL,ii);
            end
            %}
    %
%             if track==1
                %If using spherical cap assumption with known
volume
%
                if time(ii,LLL)<0.06     %assuming the droplet
doesn't move for 16 seconds
                    syms a
                    eqn = V==(1/6)*pi*a*(3*(L(ii,LLL)/2)^2 +
a^2);
                    hh(ii,LLL) = solve(eqn,a,'Real',true);
                    h(ii,LLL) = sym2poly(hh(ii,LLL));
                else
                    h(ii,LLL) = 2*V/(0.9*A(ii,LLL));
                end
                %}
%             else if track ==2
%{
                    if time(ii,LLL)<0.06    %block for
cylindrical assuumption
                        h(ii,LLL) = V/A(ii,LLL);
                    else
                        h(ii,LLL) = 2*V/(A(ii,LLL)*0.9);
                    end
                    %}
%                 end
%             end
    %         L = max(worldpts(:,2)) - min(worldpts(:,2));

            ratio(ii,LLL) = (0.9*L(ii,LLL))/h(ii,LLL);

              writeVideo(v,outline(:,:,1));
              clear validpoints ValidPoints;
        end
%
save(strcat(videosavepath,'dot',num2str(kk),'data.mat'),'time','
Validpoints');
        LLL = LLL+1;
        close(v);
        clear Validpoints;
```

```
%          track=track+1;
    end
end
%}
%% save and plot

%
save(strcat(savepath,'datapoints',num2str(kk),'.mat'),'worldpoin
ts');
save(strcat(videosavepath,'sheardata.mat'),'time','A','h','L','r
atio');
cHeader = {'time1' 'Area1' 'area2' 'area3' 'area4' 'area5'
'height1' 'h2'...
    'h3' 'h4' 'h5' 'Length1' ' L2' 'L3' 'L4' 'L5' 'L/h1'
'l/h2'...
    'l/h3' 'l/h4' 'l/h5'}; %dummy header
commaHeader = [cHeader;repmat({','},1,numel(cHeader))]; %insert
commaas
commaHeader = commaHeader(:)';
textHeader = strjoin(cHeader, ','); %cHeader in text with commas
%write header to file
fid = fopen(strcat(videosavepath,filename),'w');
fprintf(fid,'%s\n',textHeader);
fclose(fid);
%write data to end of file
xlswrite(strcat(videosavepath,filename),time,1,'A2');
xlswrite(strcat(videosavepath,filename),A,1,'B2');
xlswrite(strcat(videosavepath,filename),h,1,'G2');
xlswrite(strcat(videosavepath,filename),L,1,'L2');
xlswrite(strcat(videosavepath,filename),ratio,1,'Q2');
%      figure;
%     for ii=1:nob
%         plotpoints = worldpoints(ii);
%         plotpoints = cell2mat(plotpoints);
% %         plot(plotpoints(:,1),plotpoints(:,2));
%         plot(plotpoints(:,2),plotpoints(:,1));
%         hold on;
%         axis equal;
%     end
%     hold off;
%     plotpoints = worldpoints(1,2);
%     plotpoints = cell2mat(plotpoints);
%     plot(plotpoints(:,1),plotpoints(:,2));
%     hold on;
%     plotpoints = worldpoints(1,3);
%     plotpoints = cell2mat(plotpoints);
%     plot(plotpoints(:,1),plotpoints(:,2));
```

```
    set(gca,'YDir','reverse')
%     set(gca,'XDir','reverse')
% shear = D_vis*(ratio(26,1)-ratio(17,1))/(time(26,1)-
time(17,1))
%}
```

REFERENCES

[1] G. a. S.J.Kline, "Combined dye-streak and hydrogen-bubble visual observations of a turbulent boundary layer," *Fluid Mechanics,* pp. 223-239, 1974.

[2] J. B. T. R. M. a. G. P. Jordan M Fisher, "Application of femtosecond laser electronic excitation tagging (FLEET) velocimetry in a bladeless turbine," *Measurement Science and technology,* vol. 31, no. 6, 2020.

[3] N. M. Husen, "SKIN FRICTION MEASUREMENTS USING LUMINESCENT OIL FILMS," ProQuest, West Lafayette, 2017.

[4] L. Squire, "The motion of a thin oil sheet under the steady boundary layer on a body," *Journal of Fluid Mechanics,* vol. 11, pp. 161-179, 1961.

[5] T. L. a. B. L.G, "A study of the motion of oil films on surfaces in air flow, with application to the measurement of skin friction," *Journal of Physics E Scientific Instruments,* vol. 9, pp. 194-202, 1975.

[6] G. Bonfanti, "Development of Oil Dot Visualization Technique for Wall Shear Stress Measurement," Von Karman Institute for Fluid Dynamics, Rhode Saint Genese, Belgium.

[7] B. L. a. N. J.W, "The thin film equation," NASA Technical Report208767, 1999.

[8] H. N. J. P. M. J. D. Ruedi, "Evolution of three techniques for wall shear measurements in three-dimensional flows," *Experimental Fluids,* vol. 35, no. 5, pp. 389-396, 2003.

[9] P. B. Y. T. L. P. G. Pailhas, "Friction measurement in zero and adverse gradient boundary layer using oil droplet interferometric method," *Experimental Fuilds,* vol. 47, no. 2, pp. 195-207, 2009.

[10] R. W. J.D. Murphy, "The laser inferometer skin friction meter: a numerical and experimental study," *Journal of Physics. E: Science Instr.,* vol. 19, no. 9, p. 744, 1986.

[11] Z. Z, "A Flexible new technique for camera calibration," *IEEE Transactions on Pattern Analysis and Machine Intelligence,* vol. 22, no. 11, pp. 1330-1334, 2000.

[12] J. a. O. S. Heikkila, "A Four-step Camera Calibration Procedure with Implicit Image Correction," *IEEE International Conference on Computer Vision and Pattern Recognition,* 1997.

[13] J. Y. Bouguet, "Camera Calibration Toolbox for Matlab," *Computational Vision at the California Institute of Technology.*

[14] G. P. G. B. T. Y. Laura Villafane, "Local surface shear stress measurements from oil streaks thinning rate," *Sensors and Actuators A.,* vol. 223, pp. 31-39, 2014.

[15] E. O. O. R. H. G. Derrick O. NJOBUENWU, "Determination of contact angle from contact area of liquid droplet spreading on solid substrate," *Leonardo Electronic Journal of Particles and Technologies,* Vols. ISSN 1538-1078, no. 10, pp. 29-38, 2007.

[16] M. R., "Describing the uncertainties in Experimental Results," *Experimental Thermal and Fluid Science,* Vols. 8890043-X, no. doi 1:3-17, pp. 0894-1777, 1988.